Det Norske Videnskaps-Akademi

Geofysisk Norgeskart

GEOFYSISKE PUBLIKASJONE

VOL. 31 NO. 4 6 - 19

UNIVERSITETSFORLAGET

Geophysica Norvegica

is a journal of geophysics, issued under the auspices of the Norwegian Academy of Science and Letters

PUBLISHER

Universitetsforlaget: P. O. Box 7508, Skillebekk, Oslo 2, Norway
P. O. Box 142, Boston, Mass, 02113, U.S.A.

SUBSCRIPTION

Geophysica Norvegica (Geofysiske Publikasjoner) is published at irregular intervals. Order from the Publisher, Universitetsforlaget.

Geophysica Norvegica (Geofysiske Publikasjoner) is a series of scientific publications issued by the Norwegian Academy of Science and Letters. The Geophysical Commission appoints an editor and editorial committee.
Manuscripts for publication in *Geophysica Norvegica* should be carefully prepared (see Instructions to Author on p. 3 of the cover) and sent to the editor. The next step is the manuscript's submission to the Academy by a competent member, who is responsible for ensuring that the paper meets a sufficiently high scientific standard. (Members of the Academy are allowed to submit their own papers.) The final decision as to whether the paper should be published is taken by the editor.
Geophysica Norvegica is mainly intended as a journal for Norwegian authors, but papers from other authors may be accepted provided that the work has been carried out at a Norwegian institution or its content has a special relevance to Norway.

Uncertainties in calculated hydroxyl radical densities in the troposphere and stratosphere

I. S. A. ISAKSEN
Institute of Geophysics, University of Oslo

P. J. CRUTZEN
Aeronomy Laboratory, NOAA, Boulder, Colorado, USA;

The National Center for Atmospheric Research*
Boulder, Colorado, USA;

Department of Atmospheric Sciences
Colorado State University
Fort Collins, Colorado, USA

Isaksen, I. S. A. & Crutzen, P. J. Uncertainties in calculated hydroxyl radical densities in the troposphere and stratosphere. *Geophysica Norvegica*, Vol. 31, No. 4, 1977.

Vertical profiles of tropospheric and stratospheric densities of the hydroxyl radical and other hydrogen constituents have been calculated for 30°N, 45°N, and 60°N. The possible range of calculated hydroxyl densities is very large due to incomplete knowledge of several reactions. In particular, our information on methane oxidation appears to be insufficient; also the rate coefficient of the reaction $OH+HO_2 \rightarrow H_2O+O_2$ remains uncertain. Further, data on heterogeneous removal of HO_2 and H_2O_2 are needed. We emphasize the possible importance of hydrogen peroxide as an oxidant power after absorption in cloud drops. The uncertainty in the range of calculated OH concentrations is one decade in the stratosphere and two decades in the troposphere. There are similar or larger uncertainties in calculated concentrations of HO_2 and H_2O_2. The calculations indicate strongly very marked seasonal and latitudinal differences in the hydroxyl radical densities in the troposphere. The possible role of H_2O_2 and CH_3O_2H, especially with regard to heterogeneous reactions, is emphasized.

I. S. A. Isaksen, Institute of Geophysics, University of Oslo, P.O. Box 1022,Blindern, Oslo 3, Norway

1. INTRODUCTION

Although very few measurements have been made of the concentrations of the hydroxyl (OH) in the atmosphere, it is, nevertheless, clear that hydroxyl radicals play an important role in the chemistry of the atmosphere below 85 km. The important role of OH in the chemistry of the mesosphere was first discussed by Bates & Nicolet (1950), while Hampson (1964) drew attention to its importance in the chemistry of the stratosphere. Finally, Levy (1971) indicated that OH is also produced in the troposphere, and proposed that it would influence substantially tropospheric chemistry. The hydroxyl radical plays an important role in the odd oxygen balance of the atmosphere by a number of catalytic reactions (Bates & Nicolet 1950; Hampson 1964). On the other hand, the formation of nitric acid from NO_2 via the reaction

$$\text{R 15: } NO_2+OH(+M) \rightarrow HNO_3(+M)$$

protects ozone from otherwise larger catalytic destruction (Crutzen 1971). Furthermore, significant production and destruction of ozone may take place in the unpolluted troposphere by a sequence

* The National Center for Atmospheric Research is sponsored by the National Science Foundation.

This paper was submitted to the Norwegian Academy of Science and Letters, 22 October 1976.

of reactions initiated by the presence of methane and hydroxyl (Crutzen 1973, 1974a). In the troposphere and in the stratosphere OH is produced mainly by the set of reactions

$$\text{R 3a: } O_3 + h\nu \rightarrow O(^1D) + O_2 \quad \lambda \leq 327 \text{ nm}$$

and

$$\text{R 19a: } O(^1D) + H_2O \rightarrow 2OH$$

A great number of chemical compounds which are not removed efficiently by rain are mainly scavenged from the atmosphere by OH. This applies, for example, to methane, methyl chloride, carbon monoxide, molecular hydrogen, and to a large number of industrial gases, in particular several chlorocarbons such as $CHCl_3$ and C_2Cl_4, thereby substantially reducing the capability of these compounds to penetrate into the stratosphere. The breakdown of the compounds in the stratosphere would yield Cl and ClO, which attack ozone by catalytic reactions (Stolarski & Cicerone 1974; Wofsy & McElroy 1974; Crutzen 1974b).

On the other hand, the industrial gases CCl_4, $CFCl_3$ (fluorocarbon -11), and CF_2Cl_2 (fluorocarbon -12), which are released to the atmosphere in smaller quantities than some of the afore-mentioned chlorocarbons, do not react with OH. The total release of these gases is, therefore, likely to reach the stratosphere where they are broken down to Cl and ClO by photodissociation processes, thereby causing substantial reductions in the stratospheric ozone content (Molina & Rowland 1974; Rowland & Molina 1975). Observational evidence indicates strongly that the aforementioned chlorocarbon species with the exception of CCl_4, $CFCl_3$, and CF_2Cl_2, are removed by some chemical reactions in the troposphere, and reactions with OH are most likely. Having sufficient knowledge of atmospheric dispersion and of the global distribution of chemical constituents which react with OH only, it would in principle be possible to derive the global distribution of OH concentrations. However, this cannot be done at present because of lack of information on their global distribution. Furthermore, one can never be certain that one has not overlooked some other important process which removes a particular compound. A remarkable example of this is the case with N_2O, for which the variability of the atmospheric observations indicates a residence time in the atmosphere of about 10 years (Hahn 1975), while the only known loss processes in the atmosphere, photochemical destruction in the stratosphere, would allow a residence time of more than 100 years (Johnston & Selwyn 1975).

Carbon monoxide seems to be the only constituent for which there seem to be sufficient global data to make an attempt to estimate the global distribution of OH. However, there are still uncertainties about the diffusive properties of the atmosphere, and the possibility of significant additional loss processes besides reaction with OH cannot be ruled out (Crutzen 1976).

We will show in this article that the available kinetic information from laboratory studies is still insufficient to allow us to make reliable theoretical estimates of the prevailing OH concentrations in the troposphere. As the halocarbon industry is planning to convert its production of $CFCl_3$ and CF_2Cl_2 to that of other chlorocarbon compounds which react with OH, we recommend strongly that techniques to measure OH concentrations be urgently developed and used to measure atmospheric concentrations of OH, and that laboratory work be conducted to supply necessary detailed photochemical information so as allow reliable theoretical estimates to be made.

Calculations were performed for the latitude circles 30°, 45°, and 60° in the Northern Hemisphere. Temperature and air density data are those given by U.S. Supplement atmosphere, 1966. Water vapor mixing ratios in the troposphere were adopted from Oort & Rasmussen (1971), and ozone number densities given by Hering & Borden (1964) were adopted in these calculations.

2. UNCERTAINTIES IN PHOTOCHEMICAL INFORMATION

The chemical scheme leading to the formation and destruction of the odd hydrogen species (H, OH, HO_2, and H_2O_2) has already been discussed in a previous article (Crutzen et al. 1976). In this work we shall consider the uncertainties in several of the key reactions which determine the distribution of odd hydrogen species, and we will show their

large effect on the calculated concentrations of OH, HO_2, and H_2O_2 in the lower atmosphere. We will consider three different cases to emphasize the wide limits of uncertainties: a) all rate coefficients are chosen to give highest possible concentration of OH, HO_2, and H_2O_2; b) all rate coefficients are chosen to yield lowest possible concentrations; and c) whenever given, the values for the rate coefficients as recommended for the Climatic Impact Assessment Program were adopted (Hampson & Garvin 1975). The chemical reactions for which different rate coefficients were adopted are the following.

2.1. *Quantum yields for ozone photolysis*

The quantum yield as a function of wavelength for the yield of $O(^1D)$ in the photolysis of ozone near 310 nm:

R 3a: $O_3 + h\nu \rightarrow O(^1D) + O_2$ $\lambda \leq 327$ nm

is not yet known with sufficient accuracy. Tropopheric production of OH is especially dependent on the quantum yields for $O(^1D)$ production in the wavelength region 300-320 nm. For $\lambda < 310$ nm it is generally agreed that the quantum efficiency (α) is close to unity (Hampson 1973; Lin & DeMore 1973). For $\lambda > 310$ nm, Hampson (1973) assumed $\alpha = 0$, while Lin & DeMore (1973) give quantum efficiencies which gradually drop from 1 to 0 between 310 nm and 327 nm. Recent studies by Moortgat & Warneck (1975) show that the quantum yields are both temperature and wavelength dependent. In our estimates we have based the choice of quantum yields on the measurements by Lin & DeMore (1973), as they were recommended for use by Hampson & Garvin (1975). For case a), we decided to multiply all their quantum yields by a factor of two, but did not of course accept values larger than one. It may be added that the quantum yields obtained in this way are close to those derived by Moortgat & Warneck (1975) at room temperature. For case b), values for $\alpha = 1$ for $\lambda \leq 310$ nm and $\alpha = 0$ for $\lambda \geq 310$ nm were adopted. In case c), Lin and DeMore's quantum efficiency values were used at all wavelengths.

2.2. *The rate coefficients for reaction R 5 and R 19a*

R 5: $O(^1D) + M \rightarrow O(3P) + M$

R 19a: $O(^1D) + H_2O \rightarrow 2OH$

Reaction R 5 determines the densities of $O(^1D)$, and will therefore determine how effectively OH is produced through reaction R 19a. Recently, Davidson et al. (1975) have found both the deactivation rate coefficient k_5 and the reaction coefficient k_{19a} to be slightly, but significantly, temperature dependent, with faster rates for deactivation at lower temperature and faster rates for reaction at higher temperatures. These measurements are, however, not trivial and considerable experimental complications are encountered. Based on the information from these measurements and on previous experimental work, we assume the deactivation rate coefficient k_5 to lie between $3 \times 10^{-11} - 7 \times 10^{-11}$ cm^3 molecules^{-1} s^{-1} and for k_{19a} we chose the range $1 \times 10^{-10} - 4 \times 10^{-10}$ cm^3 molecules^{-1} s^{-1}. In conclusion we have adopted the following values for k_5 and k_{19a}:

case a): $k_5 = 3 \times 10^{-11}$, $k_{19a} = 4 \times 10^{-10}$

case b): $k_5 = 7 \times 10^{-11}$, $k_{19a} = 10^{-10}$

case c): $k_5 = 6 \times 10^{-11}$, $k_{19a} = 3 \times 10^{-10}$

(units cm^3 molecules^{-1} s^{-1})

2.3. *The rate constant of reaction R 21*

Reaction R 21 ($OH + HO_2 \rightarrow H_2O + O_2$) controls the densities of odd hydrogen species since this reaction is the main loss mecanism for odd hydrogen in most of the atmosphere. The rate constant of this reaction is not known to be better than one order of magnitude, and Hampson & Garvin (1975) give as the range of possible values 2×10^{-10} cm^3 molecule^{-1} s^{-1} $\leq k_{21} \leq 2 \times 10^{-11}$ cm^3 molecule^{-1} s^{-1}. The following values have therefore been used in our calculations: $k_{21} = 2 \times 10^{-11}$ for case a), $k_{21} = 2 \times 10^{-10}$ for case b), and $k_{21} = 6 \times 10^{-11}$ cm^3 molecule^{-1} s^{-1} for case c).

2.4. *The methane oxidation chain*

The chain of reactions R 24–R 32, starting with the reaction between methane and hydroxyl, is of great importance for the distribution of odd hydrogen, especially in the troposphere (see figure 1). The rates of several of these reactions have unfortunately never been determined in the laboratory. Depending on which reactions dominate, the decomposition of methane can therefore either

lead to the production or to the destruction of odd hydrogen (Levy 1971; Crutzen 1973; Crutzen et al. 1976). It is interesting to notice that this chain starts with the reaction with OH, and therefore with the loss of one odd hydrogen molecule. However, if the three hydrogen atoms remaining in the methyl radical are all converted to odd hydrogen species, there is a net production of two odd hydrogen molecules for each chain of reaction leading to the conversion of CH_4 to CO, H_2 and subsequently to CO_2 and H_2O. Under such conditions a chain reaction could be started leading to increasing concentration of odd hydrogen molecules. The result of such a chain of reactions could be that the equilibrium concentrations of odd hydrogen molecules were determined by their net production within the methane oxidation chain, rather than by reaction R 19 (which, however, still is the starter reaction).

We will therefore assume that in case a) there is a net production of two odd hydrogen molecules for each CH_4 molecule removed by reaction R 24. In case b), we will assume that reaction R 25 is followed by reaction R 27, and that CH_3O_2H is effectively washed out before being dissociated via reaction R 28. In this case each reaction of CH_4 with OH leads effectively to the net loss of two odd hydrogen molecules. For case c), we will adopt intermediate heterogeneous removal rates of CH_3O_2H, as will be discussed in more detail below.

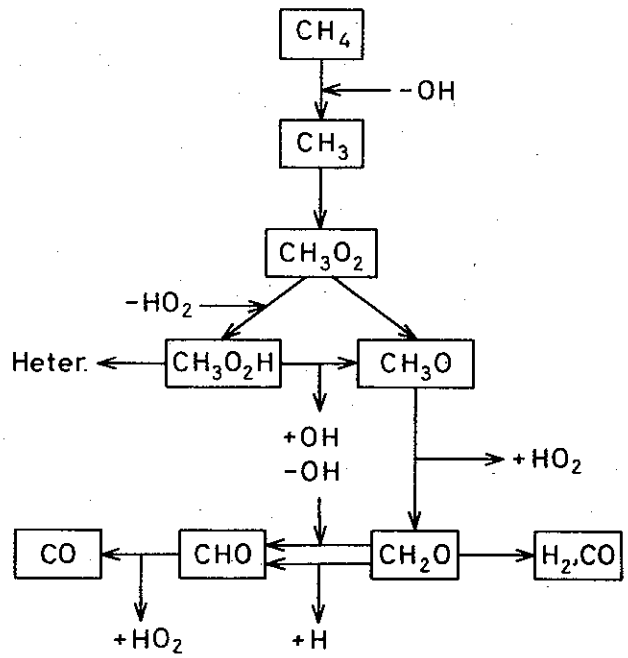

Fig. 1. A flow diagram for the expected paths in the methane oxidation chain reactions. Arrows indicate when odd hydrogen molecules (H, OH, HO_2) are either consumed (− sign) or released (+ sign).

2.5. *Heterogeneous reactions.*

Heterogeneous removal in the troposphere may play a significant role in the removal of several gases which are important for this study (Crutzen 1974a; Isaksen 1974; Crutzen et al. 1976). For instance, nitrogen oxides in the troposphere are converted to nitric acid, which together with nitrogen dioxide is removed heterogeneously by absorption in cloud droplets or attachment to aerosols, especially in the lower troposphere. Similar removal processes of H_2O_2 and CH_3O_2H could be important sinks for the odd hydrogen constituents (Isaksen 1974; Crutzen et al. 1976).

Warneck has argued that scavenging of HO_2 by aerosols in the lower troposphere will act as an effective sink for odd hydrogen by reducing recycling of OH from HO_2. By assuming that every collision between HO_2 and an aerosol particle results in scavenging, Warneck obtains lifetimes of HO_2 against heterogeneous removal of less than 10 seconds at ground level and 260 seconds at 10 km due to the presence of continental aerosol. This must certainly be considered the upper limit for aerosol scavenging of HO_2. Removal of HO_2 almost certainly does not take place at each collision and actual HO_2 residence time is therefore much longer than given above.

In our calculations we have assumed that the following species are removed heterogeneously: H_2O_2, HO_2, NO_2, HNO_3, and CH_3O_2H, with the following rates:

(case a) All heterogeneous removal was neglected.

(case b) HO_2 removal rates are based on Warneck s calculations. We have used his removal rates for continental aerosols at ground level, and converted the rates to global averages. A decrease in removal rates with height, proportional to the decrease in densities of continental aerosols with height, is used (Junge 1963). These considerations have been applied for all heights up to the tro-

popause; above the tropopause we have assumed that heterogeneous removal is negligible for all species. The heterogeneous removal rate of HO_2 in the troposphere is $h_{HO_2} = 4 \times 10^{-2} e^{-z/4\,km}$ where z is the height above ground level given in km.

For all the other compounds which are assumed to be removed heterogeneously, we have simply used rates which have height variations similar to the height variation of h_{HO_2}, but have taken collision efficiencies which are 10^{-2} of that of HO_2.

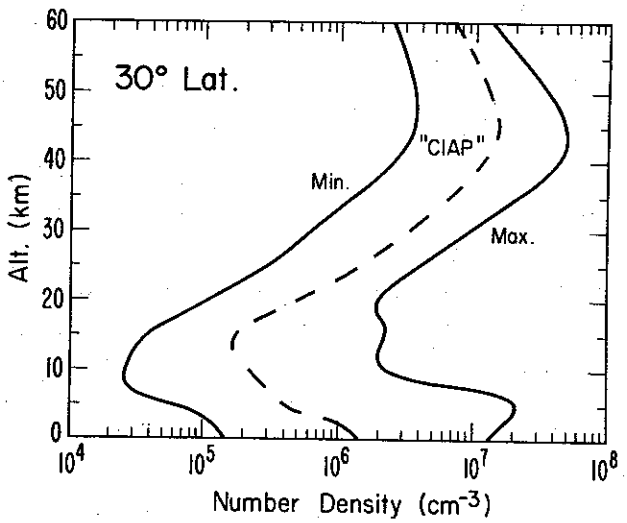

Fig. 2. Height profiles for the OH densities at 30° latitude in the Northern Hemisphere. The curves denoted Max, Min, and 'CIAP' give densities in case a), case b), and case c) respectively. The values are yearly averages over the sunlit hours.

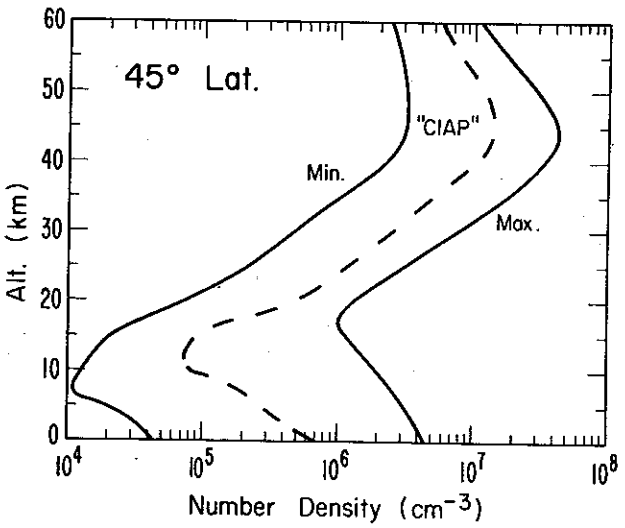

Fig. 3. The same as in Figure 2 for 45° latitude in the Northern Hemisphere.

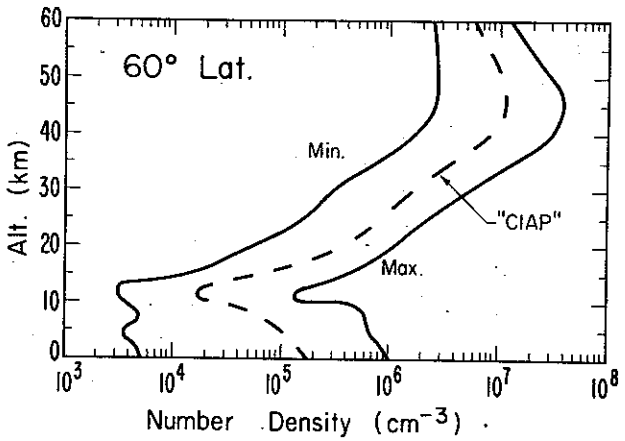

Fig. 4. The same as in Figure 2 for 60° latitude in the Northern Hemisphere.

(case c) Removal rates are assumed to be constant with height in the troposphere, and equal to 5×10^{-7} s^{-1} for all species except for HO_2, for which a rate of 5×10^{-5} s^{-1} was adopted. In the stratosphere all removal rates are set equal to zero.

3. RESULTS AND DISCUSSION

Height profiles for OH densities at 30°N, 45°N, and 60°N, are given in Figures 2, 3, and 4 respectively. These density profiles represent average values of the four seasons for sunlit hours, and the curves denoted Max, Min, and 'CIAP' depict calculated OH concentrations for case a), case b), and case c) respectively.

The very large difference between maximum and minimum values obtained at all latitudes in the troposphere (~ two decades) clearly demonstrates how sensitive the calculations are to changes in the rates discussed previously.

The poorly known detailed chemistry of the atmospheric oxidation chain (see Figure 1) is the major factor explaining these large uncertainties. We repeat that in the case of maximum OH production (case a) there is a net production of two odd hydrogen molecules following and including the reaction between CH_4 and OH. This is a typical example of a chain reaction which accelerates methane decomposition. The production of odd hydrogen by this chain is balanced by its removal via reactions R 21 and R 22.

On the other hand, the very low OH densities as calculated from case b) makes the methane oxidation chain a negligible source for odd hydrogen in the troposphere. The calculated minimum values of OH densities are low, because of the assumed large removal of odd hydrogen compounds, especially HO_2 and H_2O_2, in the troposphere (Warneck 1974; Crutzen 1974a), which prevent their conversion to OH in the troposphere. Direct reactions of OH with aerosols do not play an essential role in this context.

Differences between calculated maximum and minimum values are less pronounced in the stratosphere ($\sim$ one order of magnitude). At these heights uncertainties in the OH densities depend largely upon the rate constant of the loss reaction (R 21).

Height profiles based on the most probable values for the rates (case c) are also given in the figures. These values represent approximately the geometrical mean of the maximum and minimum values. Due to the very large calculated range in OH densities, we must consider theoretically determined tropospheric concentrations of OH to be extremely uncertain.

A comparison of densities between the three different latitudes shows a strong latitudinal dependence in calculated OH densities, for all cases in the troposphere. As we see, OH densities increase by approximately a factor of 10 going from 60° to 30° latitude. Latitudinal variations become far less pronounced in the stratosphere. Maximum values are obtained around 45 km, where the 'CIAP' model gives values in excess of $10^7/cm^3$ at all three latitude circles.

Figure 5 shows the seasonal variations of the calculated OH densities at 45° latitude according to the 'CIAP' case. Again we find the most pronounced variations in calculated OH concentrations in the troposphere.

Maximum OH densities are obtained during summer, minimum densities in winter being approximately a factor of 4 smaller. The differences in densities between spring and fall are due to the differences in observed ozone densities used in these calculations. The smaller overburden of ozone in the stratosphere in the fall as compared to spring leads to higher OH number densities in most of the troposphere, because of deeper penetration of ultraviolet radiation into the atmosphere, leading to more intensive production of $O(^1D)$ by reaction R 3a.

The calculations show similar seasonal variations in OH densities at other latitudes. As may be expected, the magnitude of the variations was found to increase going towards higher latitudes, as a result of larger seasonal dependence of the average solar zenith angles and in temperature profiles.

The marked seasonal variations in OH densities found in our calculations are expected to lead to some seasonal variations for such gases with residence times of the order of one season or less due to reactions with OH.

Seasonal variations in OH densities are calculated to be less pronounced in the statosphere, and become negligible above 50 km.

Average yearly HO_2 number densities calculated for 45°N are shown in Figure 6. The largest difference between the calculated maximum and minimum values occur also for this component in the troposphere. The uncertainty range which is approximately a factor 100 below the tropopause, increases to nearly a factor of 1000 at ground level. The reasons for this uncertainty range are identical as indicated in the discussion of OH. However, the very low calculated HO_2 densities obtained in the lower troposphere in case b) are the result of the assumed very effective direct heterogeneous removal of HO_2.

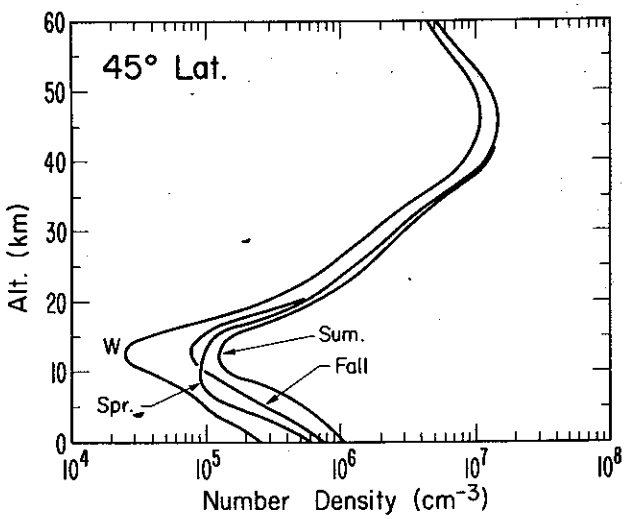

Fig. 5. Height profiles for the average diurnal OH densities at 45°N for summer, fall, winter, and spring.

In the stratosphere HO_2 density variations are similar to those of OH, which is expected as these two compounds are strongly photochemically coupled through the fast exchange reactions R 6, R 7, and R 10–R 13.

Hydrogen peroxide densities show by far the greatest sensitivity to the assumptions made about the rate constants; this is mainly due to the quadratic dependence on HO_2 concentrations by the formation reaction R 17. In case b) there would be little H_2O_2 in the troposphere. This is also partly the result of heterogeneous removal processes. Even adopting such a moderate heterogeneous removal rate as in the 'CIAP' case, heterogeneous reactions still markedly reduce the calculated H_2O_2 densities in the troposphere.

HO_2 densities show variations with latitude and season which are similar to those of OH. H_2O_2 density variations are far more pronounced. The concentrations of H_2O_2 and CH_3O_2H were found to be markedly affected by heterogeneous removal even in the 'CIAP' case. It should be noticed, in addition, that heterogeneous removal rates are meant to represent average global conditions. In the real atmosphere, conditions for such removal of H_2O_2 and CH_3O_2H will vary considerably in space and time. For instance, if clouds are present, the removal rates will increase drastically as both H_2O_2 and CH_3O_2H are water soluble gases.

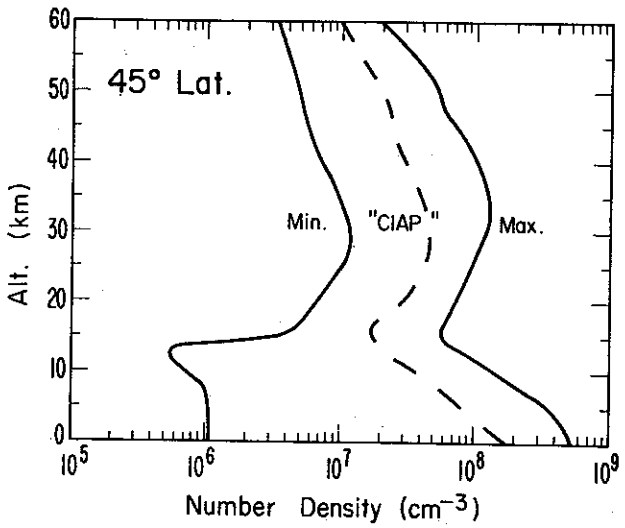

Fig. 6. Height profiles for the HO_2 densities at 45°N. The curves denoted Max, Min, and 'CIAP' give densities for case a), case b), and case c) respectively. The values are yearly averages over the sunlit hours.

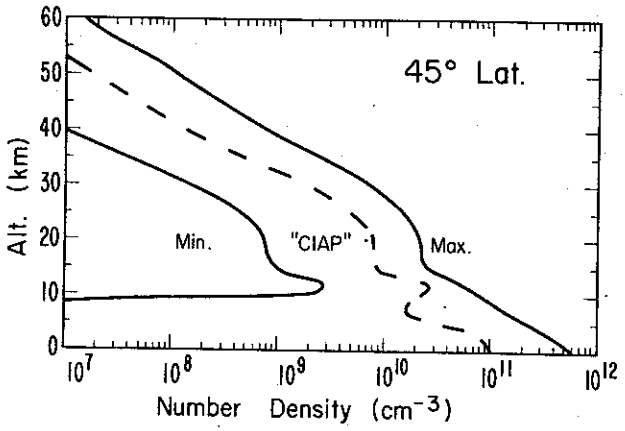

Fig. 7. The same as in Figure 6 for the H_2O_2 densities.

Under such conditions, lifetimes against rainout and washout may be only a few hours; the result will be to find locally peroxide profiles in the troposphere, similar to those found in the case of minimum values (case b). The photochemical lifetime of H_2O_2 in the troposphere is of the order of days, which means that it takes a few days for it to recover after a period of fast removal. This will in turn lead to reduced OH production by photolysis of H_2O_2. Consequently both OH and HO_2 concentrations may occasionally show considerable patchiness, in phase not only with water vapor but also with the peroxide concentrations.

If heterogeneous reactions were unimportant, we would expect H_2O_2 to be present in the lower atmosphere with volume mixing ratios of the order of 10^{-8}, which is large enough to give good hope of successful measurements. No information is available on the photochemistry of CH_3O_2H, but also this gas could attain substantial atmospheric concentrations if its abundance in the atmosphere were determined mainly by homogeneous gas phase chemistry. If, on the other hand, heterogeneous reactions of the peroxides, especially inclusion in cloud drops, do play an important role, we must consider the possibility of oxidation of a number of constituents by peroxides (e.g. SO_2 to H_2SO_4, NO and NO_2 to HNO_2 and HNO_3).

Furthermore, any rainout and washout of CH_3O_2H removes carbon from the photochemical methane oxidation chain, thereby reducing CO production rates in the atmosphere by methane oxidation. Rainfall analysis of this organic peroxide

(and its hydrolysis product CH_2O) may shed more light on this consideration. It should be mentioned that the global measurements of carbon monoxide so far obtained (Seiler 1974) are not indicative of dominating heterogeneous removal processes. We recommend strongly measurements of especially H_2O_2 in the atmosphere.

4. COMPARISON WITH MEASURED OH CONCENTRATIONS

Measured OH concentrations have been listed in Table 2 and will be compared with our calculated concentration at 30°N. There are indications, despite the substantial error bars in the measure-

Table 1. Chemical reactions. When no or very insufficient kinetic knowledge is available the reaction has been marked with an asterisk.

Oxygen reactions		
R1	$O_2+h\nu \rightarrow O+O$	$\lambda<232$ nm
R2	$O+O_2+M \rightarrow O_3+M$	$k_2=1.1\times10^{-34}\exp(500/T)$
R3a	$O_3+h\nu \rightarrow O_2+O(^1D)$	see text
R3b	$O_3+h\nu \rightarrow O_2+O$	$\lambda<1140$ nm
R4	$O_3+O \rightarrow O_2+O_2$	$ky=1.9\times10^{-11}\exp(-2300/T)$
R5	$O(^1D)+M \rightarrow O+M$	$k_5=$ see text
Reactions defining relative concentrations of OH, H, HO_2, H_2O_2, and HNO_3		
R6	$O+OH \rightarrow H+O_2$	$k_6=4.2\times10^{-11}$
R7	$O_3+OH \rightarrow HO_2+O_2$	$k_7=1.6\times10^{-12}\exp(-1000/T)$
R8	$CO+OH \rightarrow H+CO_2$	$k_8=2.1\times10^{-13}\exp(-75/T)$
R9	$H_2+OH \rightarrow H+H_2O$	$k_9=2.3\times10^{-11}\exp(-2450/T)$
R10	$O_3+H \rightarrow OH+O_2$	$k_{10}=2.6\times10^{-11}$
R11	$O_2+H+M \rightarrow HO_2+M$	$k_{11}=2.1\times10^{-32}\exp(290/T)$
R12	$O+HO_2 \rightarrow OH+O_2$	$k_{12}=2.0\times10^{-11}$
R13	$O_3+HO_2 \rightarrow OH+2O_2$	$k_{13}=1.0\times10^{-13}\exp(-1250/T)$
R14	$NO+HO_2 \rightarrow OH+NO_2$	$k_{14}=2.2\times10^{-13}$
R15	$OH+NO_2(+M) \rightarrow HNO_3(+M)$	see Crutzen (1973)
R16	$HNO_3+h\nu \rightarrow OH+NO_2$	$\lambda<546$ nm
R17	$HO_2+HO_2 \rightarrow H_2O_2+O_2$	$k_{17}=3.0\times10^{-11}\exp(-500/T)$
R18	$H_2O_2+h\nu \rightarrow OH+OH$	$\lambda<380$ nm
Production and loss reactions for odd hydrogen		
R19a	$H_2O+O(^1D) \rightarrow OH+OH$	k_{19a} see text
R19b	$CH_4+O(^1D) \rightarrow CH_3+OH$	$k_{19b}=4.0\times10^{-10}$
R19c	$H_2+O(^1D) \rightarrow H+OH$	$k_{19c}=3.0\times10^{-10}$
R20	$OH+OH \rightarrow H_2O+O$	$k_{20}=1.1\times10^{-11}\exp(-500/T)$
R21*	$OH+HO_2 \rightarrow H_2O+O_2$	k_{21} see text
R22	$OH+H_2O_2 \rightarrow H_2O+HO_2$	$k_{22}=1.7\times10^{-11}\exp(-900/T)$
R23	$OH+HNO_3 \rightarrow H_2O+NO_3$	$k_{23}=6.0\times10^{-13}\exp(-400/T)$
Methane oxidation reactions (see text)		
R24	$OH+CH_4 \rightarrow H_2O+CH_3$	$k_{24}=2.5\times10^{-12}\exp(-1660/T)$
R25	$CH_3+O_2+M \rightarrow CH_3O_2+M$	$k_{25}=2.6\times10^{-31}$
R26*	$CH_3O_2+NO \rightarrow CH_3O+NO_2$	$k_{26}=1.5\times10^{-12}\exp(-500/T)$
R27*	$CH_3O_2+HO_2 \rightarrow CH_3O_2H+O_2$	$k_{27}=3.0\times10^{-11}\exp(-500/T)$
R28*	$CH_3O_2H+h\nu \rightarrow CH_3O+OH$	$J_{CH_3O_2H}=J_{H_2O_2}$
R29*	$CH_3O+O_2 \rightarrow CH_2O+HO_2$	$k_{28}=4.2\times10^{-13}\exp(-3000/T)$
R30a*	$CH_2O+h\nu \rightarrow H_2+CO$	$\lambda\lesssim360$ nm
R30b*	$CH_2O+h\nu \rightarrow H+CHO$	$\lambda\lesssim360$ nm
R31	$CH_2O+OH \rightarrow H_2O+CHO$	$k_{31}=1.4\times10^{-11}$
R32	$CHO+O_2 \rightarrow HO_2+CO$	$k_{32}=1.7\times10^{-13}$

Nitrogen reactions

R33	$NO+O_3 \rightarrow NO_2+O_2$	$k_{33}=9.0\times10^{-13}\exp(-1200/T)$
R34	$NO_2+O \rightarrow NO+O_2$	$k_{34}=9.2\times10^{-12}$
R35	$NO_2+h\nu \rightarrow NO+O$	$\lambda<400$ nm
R36	$N+O_3 \rightarrow NO+O_2$	$k_{36}=3.0\times10^{-11}\exp(-1200/T)$
R37	$N+O_2 \rightarrow NO+O$	$k_{37}=1.1\times10^{-14}\exp(-3150/T)$
R38	$N+OH \rightarrow NO+H$	$k_{38}=5.3\times10^{-11}$
R39	$N+HO_2 \rightarrow NO+OH$	$k_{39}=2.0\times10^{-10}$
R40	$NO+h\nu \rightarrow N+O$	$\lambda<191$ nm
R41	$N+NO \rightarrow N_2+O$	$k_{41}=2.7\times10^{-11}$
R42	$N_2O+h\nu \rightarrow N_2+O$	$\lambda<337$ nm
R43a	$N_2O+O(^1D) \rightarrow NO+NO$	$k_{43a}=1.1\times10^{-10}$
R43b	$N_2O+O(^1D) \rightarrow N_2+O_2$	$k_{43b}=1.1\times10^{-10}$

(Units: Two-body reactions: cm^3 $molecules^{-1}$ s^{-1}, three-body reactions: cm^6 $molecules^{-2}$ s^{-1}.)

ments, that in the troposphere measured OH concentrations agree best with the maximum calculated OH concentrations. In the stratosphere, observed OH concentrations seem to lie between the 'CIAP' and 'Max' range. A greater number of measurements, and more accurate measurements, of OH concentrations in the atmosphere are clearly needed to make firm conclusions on the photochemistry of OH in the atmosphere, but the few observations so far obtained point towards the presence of substantial OH concentrations in the atmosphere rather close to those calculated from kinetic assumptions made in the 'Max' case.

5. CONCLUSIONS

Our calculations have first of all shown that calculated densities of the hydroxyl radical in the troposphere are sensitive to several key reactions, the rate constants of which are insufficiently known. They show strong latitudinal and temporal variations. Recent observations of OH concentrations, obtained after completion of the calculations, have already provided some guidance as to the range of possible reaction coefficients. More information is, however, very much needed.

The following main points should be kept in mind if OH concentrations are used to estimate distribution and loss rates of reactive constituents in the lower atmosphere:

a) Due to uncertain knowledge of reaction rates and the reaction routes of the methane oxidation, it is at present still only possible to give an order of magnitude estimate of OH densities in the troposphere.

b) It is seen that an extensive set of tropospheric observations must be made to establish the variability in OH concentrations with height, latitude,

Table 2. Measured concentrations of OH radicals. The tropospheric measurements were made by Davis et al. (1976) and the stratospheric measurements by Anderson (1976).

Day	Hour or zenith angle (θ)	Latitude	Altitude	OH concentration (molecules cm^{-3})
Oct. 15, 1975	12:00–14:00	32°N	7 km	$3.5\pm2.3\times10^6$
Oct. 24, 1975	12:20–14:00	21°N	7 km	$8.1\pm3.2\times10^6$
Oct. 25, 1975	12:00–14:00	21°N	11.5 km	$4.9\pm2.0\times10^6$
July 18, 1975	$\theta=80°$	32°N	40 km	$2.0\binom{+1.5}{-1.0}\times10^7$
Jan. 12, 1976	$\theta=80°$	32°N	43 km	$2.8\times10^7(\pm35\%)$
Jan. 12, 1976	$\theta=80°$	32°N	30 km	$4.5\times10^6(\pm35\%)$

and season, which were calculated to be large.

c) The non-uniformity of the heterogeneous removal rates of H_2O_2 by rainout and washout may lead to a marked patchiness in prevailing OH concentrations in the lower troposphere.

d) In the stratosphere, OH concentrations show far smaller variations with latitude and season than in the troposphere. Uncertainties in chemical reaction rates have a much smaller effect on the distribution of OH concentrations than found in the troposphere. However, due to the importance of OH in determining the rationing of ClX in ClO and HCl, accurate knowledge of OH concentrations in the stratosphere, obtained from measurements, is of fundamental importance.

REFERENCES

Anderson, J. G. 1976. *Geophys. Res. L. 3*, 165.

Bates, D. R. & Nicolet, M. 1950. *Geophys. Res. 55*, 301.

Crutzen, P. J. 1970. *Quart. J. Roy. Meteor. Soc. 96*, 320.

Crutzen, P. J. 1971. *J. Geophys. Res. 76*, 7311.

Crutzen, P. J. 1973. *Pure Appl. Geophys. 106–108*, 1385.

Crutzen, P. J. 1974a. *Tellus 26*, 47.

Crutzen, P. J. 1974b. *Can. J. Chem. 52*, 1569.

Crutzen, P. J. 1976. Proc. of the 4th CIAP Conference. Dept of Transportation, Camb. MA.

Crutzen, P. J., Isaksen, I. S. A. & McAffe, J. 1976. Submitted to *J. Geophys. Res.*

Davidson, J. A., Sadowski, C. A., Schiff, H. I., Streit, G. E., Jennings, D. A., Howard, C. J., & Schmeltekopf, A. L. 1976 Submitted to *J. Chem. Phys.*

Davis, D. D., Heaps, W., & McGee, T. G. 1976. Submitted to *Geophys. Res. L.*

Hahn, J. 1975. Meteor-Forschungsgebnisse, Reihe A, Heft 16.

Hampson, J. 1964. CARDE Report T. N. 1627/64.

Hampson, R. F. 1973. *J. Phys. Chem. Ref. Data 2*, 267.

Hampson, R. F. & Garvin, D. 1975. NBS Technical Note 866, U.S. Dept. of Commerce.

Herring, W. S. & Borden, T. S. 1964. Environmental research papers, Vol. 2, No. 38.

Isaksen, I. S. A. 1974. Inst. of Geophys., Report No. 3. University of Oslo.

Johnston, H. S. & Selwyn, G. 1975. *Geophys. Res. Lett.* 2, 549.

Junge, C. 1963. *Air Chemistry and Radioactivity.* International Geophysical Series 4, Academic Press, New York.

Levy, H. 1971. *Science 173*, 141.

Levy, H. 1972. *Planet. Space. Sci. 20*, 919.

Levy, H. 1973, *Planet. Space. Sci. 21*, 575.

Lin, C. L. & DeMore, W. B. 1973. *Photochem. 2*, 161.

Moortgat, G. K. & Warneck, P. 1975. *Z. Naturforsch. 30a*, 835.

Molina, M. J. & Rowland, F. S. 1974. *Nature 249*, 810.

Oort, A. H. & Rasmussen, E. M. 1971. NOAA, professional paper 5, U.S. Dept. of Commerce, Rockville, Md.

Rowland, E. S. & Molina, M. J. 1975. *Rev. Geophys. Space Phys. 13.*

Seiler, W. 1974. *Tellus 26*, 116.

Stolarski, R. S. & Cicerone, R. J. 1974. *Can. J. Chem. 52*, 1510.

Warneck, P. 1974. *Tellus 26*, 39.

Wofsy, S. C. & McElroy, M. B. 1974. *Can. J. Chem. 52*, 1582.

A simplified method to include molecular scattering and reflection in calculations of photon fluxes and photodissociation rates

IVAR S. A. ISAKSEN, KNUT HELGE MIDTBØ & JENS SUNDE
Institute of Geophysics, University of Oslo

PAUL J. CRUTZEN
Aeronomy Laboratory, NOAA, Boulder, Colorado
National Center for Atmospheric Research,* Boulder, Colorado, U.S.A.

Isaksen, I. S. A., Midtbø, K. H., Sunde, J. & Crutzen, P. J. A simplified method to include molecular scattering and reflection in calculations of photon fluxes and photodissociation rates. *Geophysica Norvegica*, Vol. 31, No. 5, 1977.

Solar fluxes in the wavelength interval 200 to 750 nm have been calculated at height intervals of 1 km in the atmosphere below 50 km for three different solar zenith angles: 30°, 60°, and 85°. Attenuation by molecular oxygen ($\lambda<380$ nm and $\lambda>440$ nm), scattering by air molecules, and reflection by the Earth's surface are included in the calculations. The scattering is accounted for in a simplified way: it is assumed that one half of the radiation proceeds in the direction of the direct beam, the other half goes in the opposite direction. In this way up to five orders of scattering were taken into account. This computationally simple and relatively 'inexpensive' method is shown to approximate the exact method of radiative fluxes within a few percent accuracy for virtually all conditions which are of photochemical importance in the atmosphere. Dissociation rates for the gases O_3, CH_2O, H_2O_2, NO_2, NO_3, HNO_3, N_2O_5, N_2O, and $ClONO_2$ are calculated as a function of height and solar zenith angle. The effect of scattering and reflection in photochemical calculations of the distribution of a number of gases is found to depend markedly on the wavelength region where dissociation takes place.

I. S. A. Isaksen, Institute of Geophysics, University of Oslo, P.O. Box, 1022, Blindern, Oslo, 3, Norway

1. INTRODUCTION

To describe accurately the photochemistry of the lower atmosphere with the aid of models it is important to incorporate the effect of solar radiation processes in the models in a realistic way. In calculations in the upper stratosphere and mesosphere, sufficient accuracy is obtained for most purposes by considering the attenuation as due only to absorption by O_2 and O_3 alone, with a few important exceptions that will be discussed in this paper.

In the lower troposphere molecular scattering markedly reduces the incoming solar radiation in the UV and visible region. Calculation of solar fluxes is complicated by the fact that the spectral region of special interest for tropospheric chemistry, the wavelength region 290–330 nm, where excited state atomic oxygen ($O(^1D)$) is produced, is a transition region, where both ozone absorption and molecular scattering take place. At shorter wavelength, ozone absorption dominates, and at longer wavelength molecular scattering dominates.

Tropospheric chemistry normally deals with conditions which vary markedly over a relatively

This paper was submitted to the Norwegian Academy of Science and Letters, 22 October 1976.

* The National Center for Atmospheric Research is sponsored by the National Science Foundation.

short time. For large solar zenith angles the chemistry will in such situations depend critically on the molecular scattering.

Accurate calculations of the solar fluxes due to ozone absorption and molecular scattering have been given by several authors (e.g. Luther & Gelinas 1976, Sundararaman et al. 1975). Such models are rather complicated and time consuming, and are therefore not easily incorporated in time dependent photochemical models.

In this paper we will discuss a simplified model where molecular scattering and reflection due to the Earth's albedo are included in the solar flux calculations. The calculations are based on the assumption that all scattering takes place in the direction of the sun's radiation, with one half scattered toward the sun, and the other half away from the sun. It is found to be sufficient to include scattering up to the 5th order. The calculations are further simplified by using constant height intervals ($\Delta z = 1$ km), rather than constant optical thickness. A simplified version of this procedure has previously been used to obtain heating rates from NO_2 absorption of photon fluxes (Hesstvedt & Isaksen, 1974).

We will show that the accuracy in the calculation of solar fluxes is greatly improved when compared with models where absorption by O_2 and O_3 are assumed to be the only attenuation agent in the atmosphere. Profiles for solar dissociation rate constants of O_3, CH_2O, H_2O_2, NO_2, NO_3, HNO_2, HNO_3, N_2O, N_2O_5, and $ClONO_2$ will be presented (with and without the consideration of multiple molecular scattering).

2. SOLAR FLUXES

Solar fluxes are calculated in the spectral region 200–750 nm, at height intervals $\Delta z = 1$ km, extending from the ground and up to 50 km. Above

Table 1. Ozone number densities and ozone column densities used in the model. The numbers in parenthesis give the power of 10.

z km	O_3 number density $cm^{-3} \times 10^{-11}$	O_3 column density cm^{-2}	z km	O_3 number density $cm^{-3} \times 10^{-11}$	O_3 column density cm^{-2}
50	1.2	6.00 (16)	24	35.6	3.54
49	1.4	7.30	23	38.3	3.91
48	1.8	8.90	22	40.9	4.31
47	2.2	1.09 (17)	21	44.9	4.73
46	2.8	1.34	20	48.8	5.20
45	3.6	1.66	19	50.7	5.70
44	4.5	2.07	18	52.5	6.21
43	5.2	2.55	17	47.7	6.71
42	6.2	3.12	16	42.9	7.17
41	7.5	3.80	15	39.3	7.58
40	9.2	4.64	14	35.6	7.95
39	10.7	5.63	13	32.7	8.29
38	12.5	6.79	12	29.8	8.60
37	14.7	7.15	11	21.8	8.86
36	16.2	8.69	10	13.8	9.04
35	17.0	1.04 (18)	9	10.4	9.16
34	17.7	1.21	8	7.00	9.25
33	18.1	1.39	7	7.50	9.32
32	18.5	1.57	6	7.90	9.40
31	19.1	1.76	5	8.00	9.48
30	19.8	1.95	4	8.00	9.56
29	21.3	2.16	3	7.60	9.64
28	23.2	2.38	2	7.10	9.71
27	25.7	2.63	1	7.10	9.78
26	28.5	2.90	0	7.10	9.85 (18)
25	32.1	3.20			

50 km, molecular scattering is negligible; it can therefore be assumed that the incoming solar radiation reaching 50 km is weakened by absorption only, which is due to O_2 ($\lambda < 242$ nm) and O_3 ($\lambda < 380$ nm and $\lambda > 440$ nm). Height profiles of the total air densities (M) and of O_2 are taken from the US Supplement Atmosphere 1966 for 50° Summer in the Northern Hemisphere. The adopted O_3 profile is given in Table 1, along with ozone column densities.

Molecular scattering depends strongly on the wavelength of the radiation (proportional to λ^{-4}), and if we define the scattering angle (the angle between the direction of the incoming solar beam and the scattered radiation) as θ, the intensity of the scattered radiation in different directions is proportional to $1+\cos^2\theta$. Even if the scattering is substantial in all directions, it is seen from this expression that it is more pronounced along the direction of the sun's radiation than it is in other directions. We will therefore try to simplify the calculations of scattered radiation by considering all scattering to take place in the direction of the sun's beam, with half of the radiation scattered backwards toward the sun and the other half away from the sun, and we will explore the accuracy of the computational method.

The attenuation of the direct solar radiation due to molecular scattering can be considered in the same way as attenuation by O_2 and O_3. The direct incoming solar flux (here given by the superscript o) at a certain wavelength, reaching a height level i, is, according to Beer's law:

$$\downarrow F_i^o = \downarrow F_{i+1}^o \cdot \exp(-\Delta\tau^*_{i+1/2}) \qquad (1)$$

This equation gives the reduction in flux from the level above $(i+1)$ to the level we consider. $i+\frac{1}{2}$ refers to the height interval i to $i+1$, and $\Delta\tau^*_{i+1/2}$ is the total optical depth in this height interval, which is given by the absorption by O_2 and O_3 and by the scattering by air molecules (M):

$$\Delta\tau^*_{i+1/2} = (\sigma_{O_2}[O_2]_{i+1/2} + \sigma_{O_3}[O_3]_{i+1/2} + \sigma_R \cdot [M]_{i+1/2}) \cdot \Delta z \cdot F(\theta) \qquad (2)$$

σ_{O_2}, σ_{O_3}, and σ_R are the absorption coefficients of O_2, O_3, and the Rayleigh scattering coefficient respectively, and $[O_2]_{i+1/2}$, $[O_3]_{i+1/2}$, and $[M]_{i+1/2}$ are the average densities of O_2 and M respectively in the height interval i to $i+1$, and are represented by their arithmetic mean values. Δz is the height interval (10^5 cm), and $F(\theta)$ is a function of the solar zenith angle θ. For $\theta \leq 75°$, $F(\theta)$ is equal to $1/\cos\theta$, while it is represented by the Chapman function for $\theta > 75°$.

At the upper boundary ($i=51$), where attenuation of the direct incoming solar radiation is due to absorption only, the flux is given by:

$$\downarrow F_{51}^o = \downarrow F_\infty^o \exp(-(\sigma_{O_2}[O_2]_{51} \cdot HO_2 + \sigma_{O_3} \cdot [O_3]_{51} \cdot HO_3) F(\theta)) \qquad (3)$$

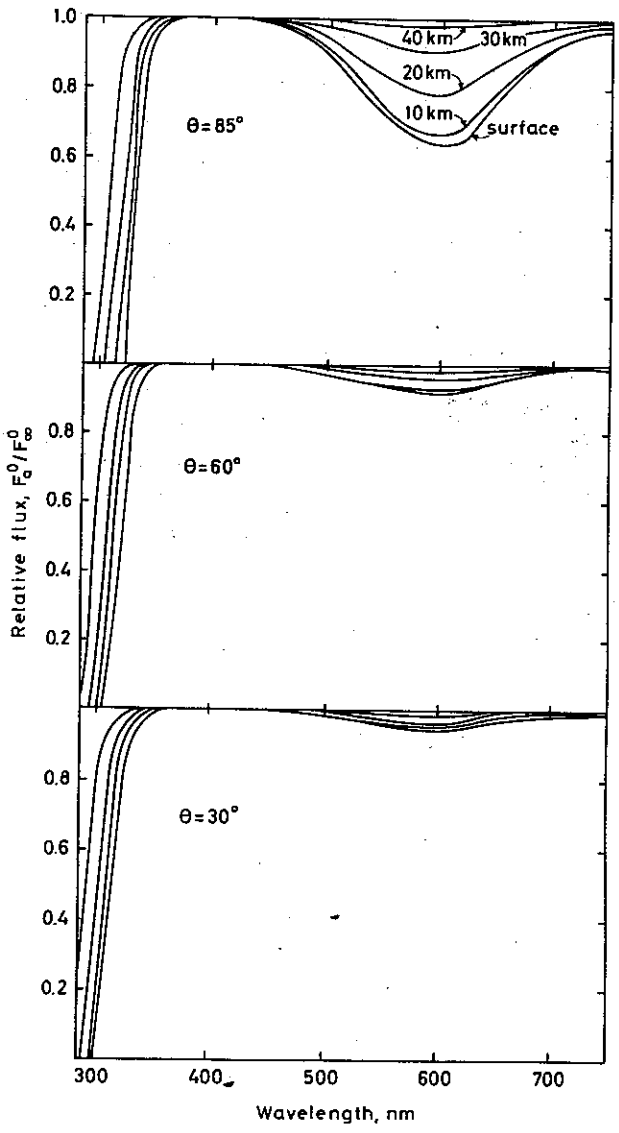

Fig. 1. Relative photon flux $\downarrow F_a^0/F_\infty^0$ versus wavelength for height levels 40 km, 30 km, 20 km, 10 km, and 0 km, at different solar zenith angles θ. Definition of $\downarrow F_a^0$ and F_∞^0 is given in the text.

$\downarrow F^o_\infty$ is the extraterrestrial solar flux, and HO_2 and HO_3 the adopted scale heights of O_2 (7×10^5 cm) and O_3 (5×10^5 cm) at 50 km respectively.

It is convenient to express the fluxes reaching an arbitrarily height level i (eq. (1)) in terms of the flux reaching the upper boundary as given by eq. (3). By substituting for $\downarrow F^o_{i+1}$ in eq. (1), $\downarrow F^o_i$ can eventually be expressed by the flux reaching height level $i=51$:

$$\downarrow F^o_1 = \downarrow F^o_{51} . \exp\left(-\sum_{j=i+1}^{51} \Delta\tau^*_{j-1/2}\right) \qquad (4)$$

where the subscript $j-\frac{1}{2}$ refers to the height level $j-1$ to j; the summation therefore gives optical thickness between height level i and height level 51. In order to show the effect of ozone absorption on the solar fluxes for $\lambda \geq 285$ nm, the ratio $\downarrow F^o_a / F^o_\infty$ is given in Figure 1. $\downarrow F^o_a$ is obtained from an expression similar to eq. (4), where attenuation of the fluxes is due to ozone absorption only. $\downarrow F^o_\infty$ is the incoming extraterrestrial solar flux. For $\lambda < 285$ nm the photon fluxes are effectively absorbed by ozone (and by molecular oxygen for $\lambda < 242$ nm). We notice the marked cut-off in solar fluxes reaching the lower atmosphere for wavelengths around 300 nm, depending on height and solar zenith angle. In the wavelength region of the Chappuis bands, between approximately 500 and 700 nm, ozone absorbs only moderately at solar zenith angles up to 60° (<10%). At solar zenith angles of 85°, however, the photon fluxes reaching the troposphere may be markedly reduced (~30% at 600 nm).

The reflected direct solar radiation due to the Earth's albedo, reaching the height level i from below, is given by an expression analog to eq. (1):

$$\uparrow F^o_i = \uparrow F^o_{i-1} \exp\left(-\Delta\tau^*_{i-1/2}\right) \qquad (5)$$

$\uparrow F^o_{i-1}$ refers to the reflected direct solar radiation reaching the height level below $(i-1)$ the level considered, and $i-\frac{1}{2}$ refers to the height interval $i-1$ to i.

The direct incoming solar radiation reaching the surface of the Earth is obtained from eq. (4):

$$\downarrow F^o_1 = \downarrow F^o_{51} \exp\left(-\sum_{j=2}^{51} \Delta\tau^*_{j-1/2}\right) \qquad (6)$$

For a surface albedo equal to A, the reflected flux of the direct solar radiation reaching the height level i is given by:

$$\uparrow F^o_i = \downarrow F^o_1 . A . \exp\left(-\sum_{j=1}^{i-1} \Delta\tau^*_{j+1/2}\right) \qquad (7)$$

The direct incoming and reflected solar radiation is then given by

$$F^o_i = \downarrow F^o_i + \uparrow F^o_i \qquad (8)$$

Expressions for the scattered fluxes of different orders are obtained in the following way: first order fluxes are expressed in terms of the direct solar fluxes as given by equations (4) and (7). The second order scattered fluxes are then obtained from expressions containing first order scattered fluxes only. Similarly all scattered fluxes of higher orders are given by fluxes of lower orders. Let us consider the scattered flux of n^{th} order reaching a height level i. The downward component can be considered as the sum of the flux of the order $n-1$ which is scattered downward in the height interval above level i, and the downward flux of the order n scattered at higher height intervals. The equation takes the form:

$$\downarrow F^n_i = [\tfrac{1}{2}(\downarrow F^{n-1}_{i+1} + \uparrow F^{n-1}_i).(1-\exp(-\Delta\tau_{i+1/2})) + \downarrow F^n_{i+1}] . \exp\left(-\Delta\tau^*_{i+1/2}\right) \qquad (9)$$

$\Delta\tau_{i+1/2}$ is the optical depth of air in the height interval i to $i+1$, defined in a way similar to the total optical depth (eq. (2)). The factor $\frac{1}{2}$ before the fluxes of order $n-1$ arises from our assumption that half the scattered radiation is downward along the direction of the sun's beam.

An expression similar to eq. (9) can be used to eliminate the term $\downarrow F^n_{i+1}$. This procedure can be repeated until scattered fluxes of the order n for all levels between level i and the upper boundary are eliminated. At the upper boundary all downward scattered fluxes are assumed to be equal to zero. Hence, the downward scattered fluxes of the order n at a height level i can be expressed by fluxes of the order $n-1$.

Eq. (9) will then take the form:

$$\downarrow F^n_i = \sum_{j=i}^{50} [\tfrac{1}{2}(\downarrow F^{n-1}_{j+1} + \uparrow F^{n-1}_j).(1-\exp(\Delta\tau_{j+1/2}))] \times \exp\left(-\sum_{k=j}^{i} \Delta\tau^*_{k+1/2}\right) \qquad (10)$$

The upward component of the scattered flux of nth order, reaching the height level i, is obtained in a way similar to the downward component reaching the same level (eq. (9)). It is given by the sum of the fluxes of the order $n-1$, which is scattered upwards at the height interval below the level i, and of the order n scattered upwards at all lower levels.

$$\uparrow F_i^n = [\tfrac{1}{2}(\uparrow F_{i-1}^{n-1} + \downarrow F_i^{n-1}) . (1 - \exp(-\Delta\tau_{i-1/2})) + \uparrow F_{i-1}^n] . \exp(-\Delta\tau_{i-1/2}^*) \quad (11)$$

$\Delta\tau_{i-1/2}$ is the optical depth of air in the height interval $i-1$ to i. Following the same procedure as we did in the cases of the downward flux (eq. (10)), the term $\uparrow F_{i-1}^n$ can be eliminated to give terms containing fluxes of the order $n-1$ only for height levels between level i and lower boundary. At the lower boundary, however, there is an upward scattered flux of the order n due to reflection at the Earth's surface. Eq. (11) will then take the form:

$$\uparrow F_j^n = \sum_{j=2}^{i} [\tfrac{1}{2}(\uparrow F_{j+1}^{n-1} + \downarrow F_j^{n-1}) . (1 - \exp(-\Delta\tau_{j-1/2}))] \times \exp(-\sum_{k=j}^{i} \Delta\tau_{k-1/2}^*) + \downarrow F_1^n . A . \exp(-\sum_{j=2}^{i} \Delta\tau_{j-1/2}^*) \quad (12)$$

Hence, the upward scattered flux of the order n reaching a height level i is expressed by fluxes of the order $n-1$.

The flux of the order n reaching the height level i is given by:

$$F_i^n = \downarrow F_i^n + \uparrow F_i^n \quad (13)$$

We find that scattered fluxes above the fifth order have negligible effects on the total fluxes, the total flux reaching a height level i is therefore given by the equation:

$$F_i = F_i^0 + \sum_{n=1}^{5} F_i^n \quad (14)$$

Sundararaman et al. (1975) have estimated the downward component of the diffusive flux relative to the direct incoming solar flux which reaches the Earth's surface, by solving the equation of radiative transfer. This provides us with a good opportunity to test the accuracy of our simplified flux calculations. At the Earth's surface the downward component of the scattered flux is obtained from the expression of the total scattered flux:

$$F_{D1} = \sum_{n=1}^{5} F_1^n \quad (15)$$

with $A = 0$.

The direct incoming solar flux at ground level is given by equation (6).

Figure 2 gives a comparison of the calculated ratio F_{D1}/F_1^0 in this work, and in the work by Sundararaman et al. (1975) for the two solar zenith angles $\theta = 30°$ and $\theta = 60°$. The comparison is made for the same total ozone density of 350 Dobson Units. The relative fluxes obtained by Sundararaman et al. in their model above approximately 300 nm for both solar zenith angles, are well reproduced in our calculations; in fact, the differences are only a few %. Below 300 nm, however, there seems to be a larger discrepancy, especially for a solar zenith of 30°. As we proceed to shorter wavelengths our model seems to overestimate the scattered fluxes. This is, however, of no significance for the

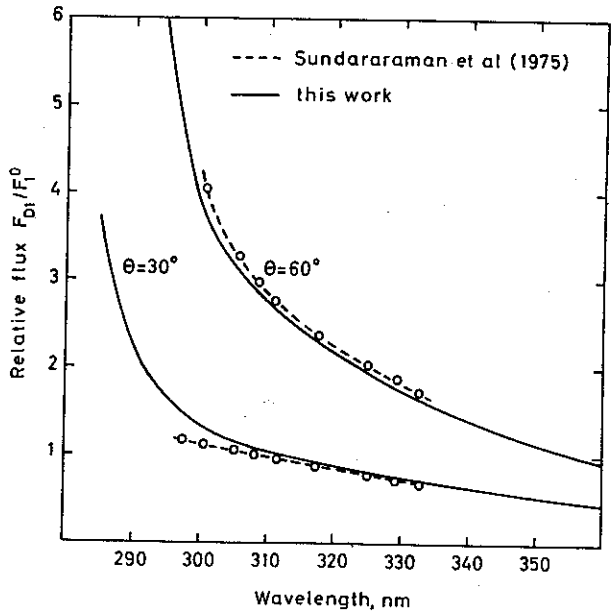

Fig. 2. The ratio of the downward multiple scattered flux F_{D1} to the direct incoming solar flux F_1^0 versus wavelength at ground level for the two solar zenith angles of 60° and 30°. The curves denoted Sundararaman et al. (1975) are taken from their tabulated values of the same ratio for an ozone column density of 350 D.U. For $\theta = 30°$ the numbers are derived at by interpolation between the solar zenith angles 25° and 40° in their Table.

dissociation rates of the different gases we consider; the strong absorption by ozone reduces the solar fluxes effectively below approximately 300 nm (see Figure 1). Finally, it should be mentioned that even if we have the same total amount of ozone as Sundararaman et al., we have a quite different vertical distribution; this might explain some of the discrepancy at shorter wavelengths where ozone absorption is strongest.

To illustrate the effect of multiple scattering on the photon fluxes reaching the lower atmosphere, we will give the fluxes obtained through equation (14) relative to the fluxes of the direct solar radiation where absorption only is considered. This

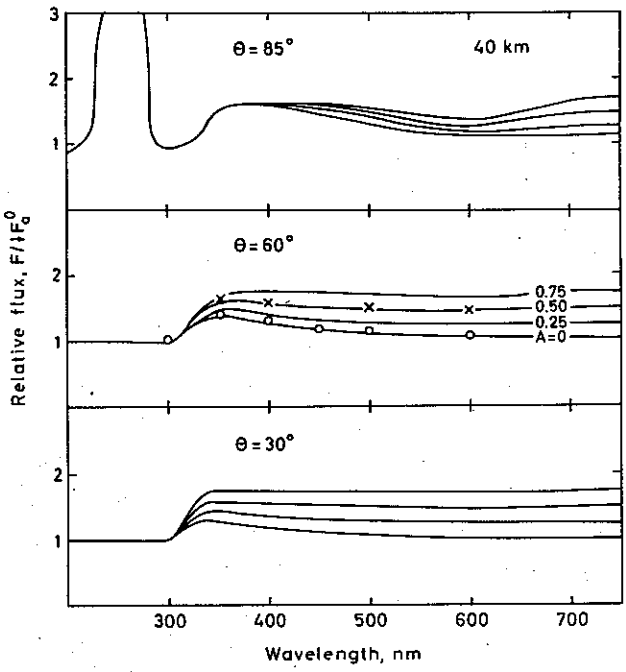

Fig. 3a

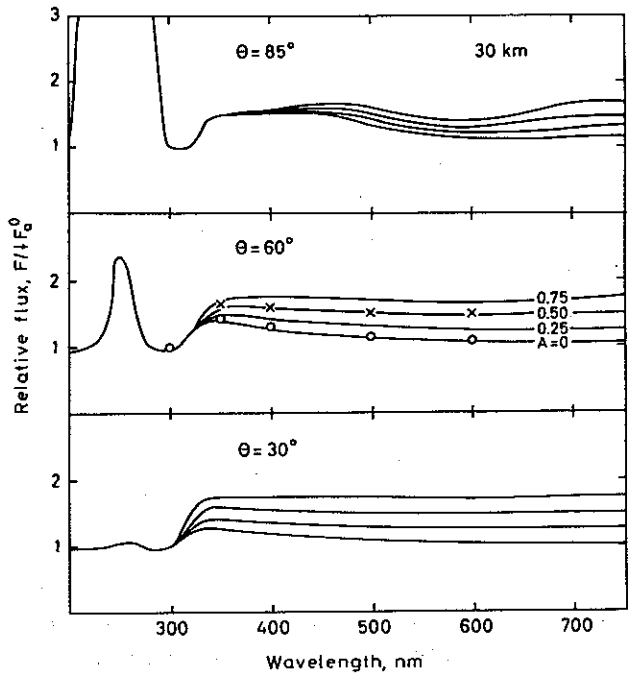

Fig. 3b

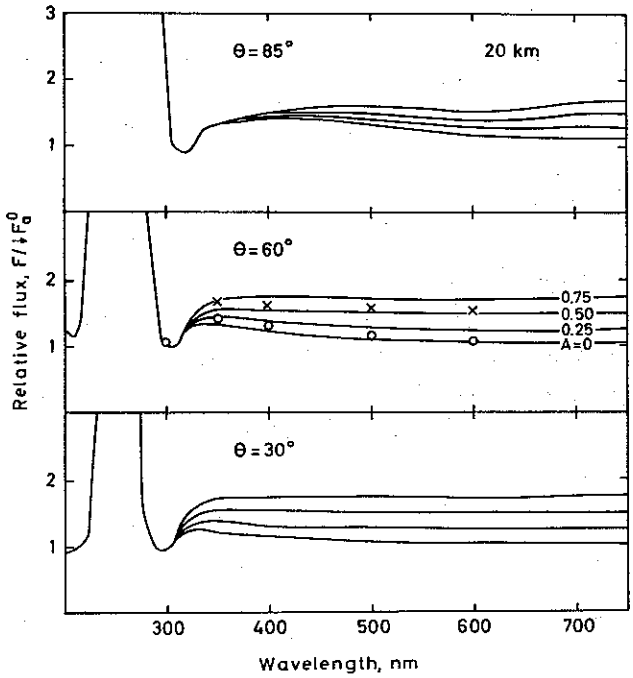

Fig. 3c

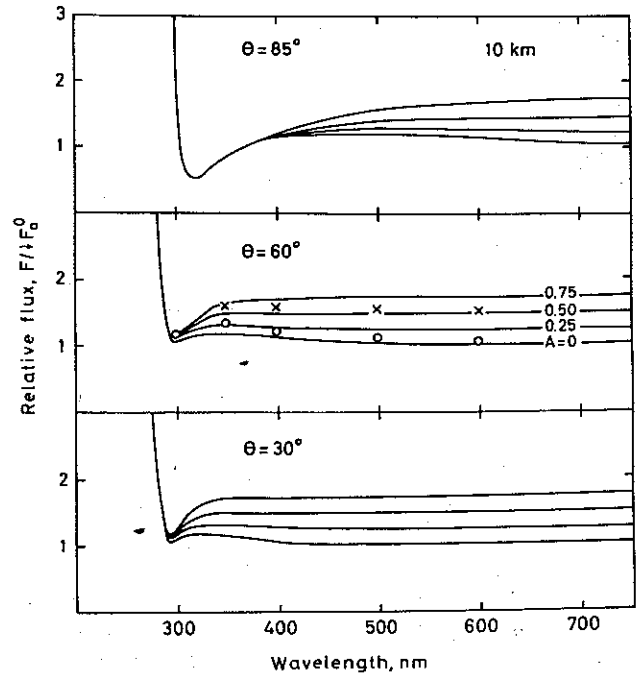

Fig. 3d

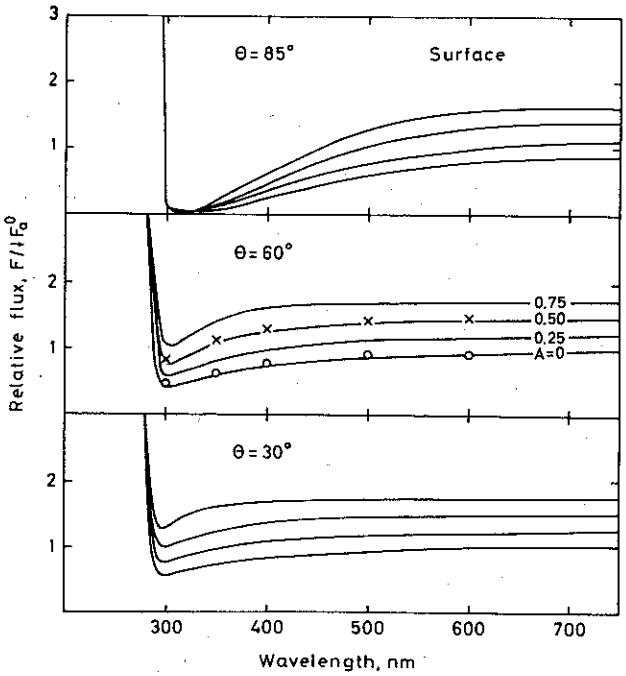

Fig. 3e

Fig. 3a–e. The ratio of the total photon flux F (multiple) scattering included) to the flux due to pure absorption $\downarrow F_a^0$ (for definition of F and $\downarrow F_a^0$ see text) versus wavelength for the different heights 40 km[a], 30 km[b], 20 km[c], 10 km[d], and 0 km[e] at different solar zenith angles θ and surface albedos A. The numbers given by O and × give the same flux ratios for albedos equal to 0 and 0.5 respectively obtained by Luther & Gelinas (1976).

presentation is the same as Luther & Gelinas (1976) used and we will compare our results with the fluxes they obtained in their calculations, using a more complete method for solving the equation of radiative transfer. The relative flux reaching a height level i is given by the equation:

$$F_{Ri} = F_i / \downarrow F_{ai}^o \qquad (16)$$

$\downarrow F_{ai}^o$ is the flux obtained in a pure absorbing atmosphere, and is obtained from an equation similar to equation (4):

$$\downarrow F_{ai}^o = \downarrow F_{51}^o \cdot \exp\left(-\sum_{j=i+1}^{51} \Delta\tau_{j-1/2}^a\right) \qquad (17)$$

$\Delta\tau_{j-1/2}^a$ is the optical depth of the absorbing atmosphere in the height interval $j-1$ to j, and is given by an expression similar to eq. (2), the difference being that the term containing Rayleigh scattering is omitted.

Figures 3*a*–3*e* give the calculated relative fluxes for each 10 km height level between 40 km and the ground, at different solar zenith angles (85°, 60°, and 30°), and with different values for the ground reflection (0·0, 0·25, 0·50, and 0·75). The calculations are done at steps of 5 nm between 200 nm and 750 nm. Luther and Gelinas have given their fluxes at a solar zenith angle of 60°. For comparison, we have also included in the figures their results for a surface albedo of 0·0 and 0·5.

It is clearly seen from the figures that the effects of molecular scattering and of ground reflection on the photon fluxes depend strongly on the wavelength and on the solar zenith angle. Below approximately 300 nm, the strong absorption by ozone effectively prevents any radiation reflected at ground from reaching the upper troposphere and stratosphere. Molecular scattering, on the other hand, strongly increases the fluxes at large optical depth. This is shown on the figure at a solar zenith angle of 85° in the middle and upper stratosphere (30 km and 40 km) and at all solar zenith angles at lower heights. Total fluxes are, however, strongly reduced in these cases; the increase in relative fluxes is therefore of limited atmospheric interest.

Above approximately 300 nm, ozone absorption is sufficiently weak to allow both molecular scattering and ground reflection to affect photon fluxes in the lower atmosphere. Since most of the total air mass is located below 10 km in the atmosphere, molecular scattering will mainly take place below this height, except for a larger solar zenith angle ($\theta = 85°$), where there also is a substantial scattering above 10 km for $\lambda < 400$ nm. This means that at all height levels from 10 km and up, molecular scattering increases the relative fluxes. Due to the wavelength dependence of molecular scattering, the relative fluxes increase with decreasing wavelength, reaching a maximum at a certain wavelength. Below, the relative fluxes decrease, a result of increasing ozone absorption. The wavelength where scattering has its maximum effect on the photon fluxes depends on the optical depth, varying from 330 nm to 400 nm. The largest increase in relative fluxes is found in the upper stratosphere at large solar angles, where it might exceed 50%.

At ground level, molecular scattering is found always to reduce the photon fluxes. It is seen that

it has a pronounced effect on the fluxes reaching ground, especially toward shorter wavelengths. At a solar zenith angle of 30°, the fluxes reaching ground at 300 nm are reduced with approximately 40%; at an angle of 60° the reduction is 60% at the same wavelength, and at a solar zenith angle of 85° no flux will essentially reach the ground at a wavelength of 300 nm.

The effect of the Earth's albedo is most pronounced in the troposphere where a large albedo strongly increases the fluxes at wavelengths above approximately 280 nm (Figure 3*e*). It is seen that the effect of the Earth's albedo at all heights above ground level depends on the solar zenith angle. At an angle of 85° hardly any increase in the fluxes is found for wavelengths less than 400 nm. At solar zenith angles of 30° and 60°, ground reflection effects the photon fluxes above approximately 320 nm. We should also notice that ozone absorption in the Chappius bands markedly reduces the reflected photon fluxes in the upper stratosphere at large solar zenith angles.

A comparison with Luther & Gelinas (1976) calculated fluxes shows in general a good agreement, both when molecular scattering only is considered, and when scattering and ground reflection ($A = 0{\cdot}5$) are considered. At ground level and in the stratosphere our calculated photon fluxes between 300 nm and 600 nm differ only a few per cent from those obtained by Luther & Gelinas. At 10 km, and to some extent also at 20 km, our method seems to underestimate the relative fluxes in the wavelength region 300 to 400 nm. Fortunately, the upper troposphere and lower stratosphere ($z \sim$ 10–20 km) is a region of relatively little interest with regard to dissociation of chemical compounds. In the regions of prime concern – the lower troposphere with regard to pollution chemistry and the upper stratosphere ($z > 20$ km) with regard to the ozone depletion problem – our model seems to give a rather good description of the effects of molecular scattering and ground reflection.

3. PHOTODISSOCIATION

Based on the fluxes obtained in eq. (14), the dissociation rate of a species n reaching a height level i is given by

$$J_{ni} = \sum_{\lambda=\lambda_1}^{\lambda_2} \alpha_{n\lambda} \cdot \sigma_{n\lambda} \cdot F_{\lambda i} \cdot \Delta\lambda \qquad (18)$$

where α_n is the quantum efficiency in dissociating the compound n, and F_i the total solar flux reaching the height level i. All values are average values in the spectral interval ($\Delta\lambda$) considered, and except for dissociation of ozone in the spectral region 300 to 327 nm, where intervals of 2 nm are used, intervals of 5 nm are used. In most cases a quantum efficiency equal to one has been applied, with some exceptions which will be discussed below.

Table 2. Photodissociation scheme

R1	$O_3 + h\nu \rightarrow O_2 + O(^1D)$	$\lambda < 300$ nm
R2	$O_3 + h\nu \rightarrow O_2 + O(^1D)$ α $\rightarrow O_2 + O(^3P)$ $1-\alpha$	300 nm $> \lambda >$ 330 nm
R3	$O_3 + h\nu \rightarrow O_2 + O(^3P)$	$\lambda > 330$ nm
R4	$NO_2 + h\nu \rightarrow NO + O$	$\lambda < 415$ nm
R5	$ClONO_2 + h\nu \rightarrow ClO + NO_2$	$\lambda < 470$ nm
R6	$N_2O + h\nu \rightarrow N_2 + O$	$\lambda < 320$ nm
R7	$HNO_2 + h\nu \rightarrow OH + NO$	$\lambda < 395$ nm
R8	$HNO_3 + h\nu \rightarrow OH + NO_2$	$\lambda < 360$ nm
R9	$NO_3 + h\nu \rightarrow NO_2 + O$	$\lambda < 580$ nm
R10	$N_2O_5 + h\nu \rightarrow NO_2 + NO_3$	$\lambda < 380$ nm
R11	$H_2O_2 + h\nu \rightarrow OH + OH$	$\lambda < 380$ nm
R12	$CH_2O + h\nu \rightarrow CHO + H$	$\lambda < 360$ nm
R13	$\rightarrow H_2 + CO$	$\lambda < 360$ nm

In the case of ozone dissociation, the quantum efficiency for excited state atomic oxygen formation (reaction R1 in Table 2) is of importance for the chemistry of the troposphere (Warneck 1975, Crutzen et al. 1976, Isaksen & Crutzen 1976). Below 300 nm it is believed to be unity, while in the wavelength region 300–327 nm it is still questionable (Lin & De More 1973, Johnston 1973, Moortgat & Warneck 1975). We have adopted the same values for the quantum efficiencies and absorption coefficients of O_3 as Crutzen et al. 1976.

The quantum efficiency of NO_2 dissociation around 400 nm is strongly wavelength dependent. Since absorption cross sections are close to their maximum values at these wavelengths, the quantum efficiencies used are of importance for the dissociation rates of NO_2. We have applied the values for dissociation rates and quantum effi-

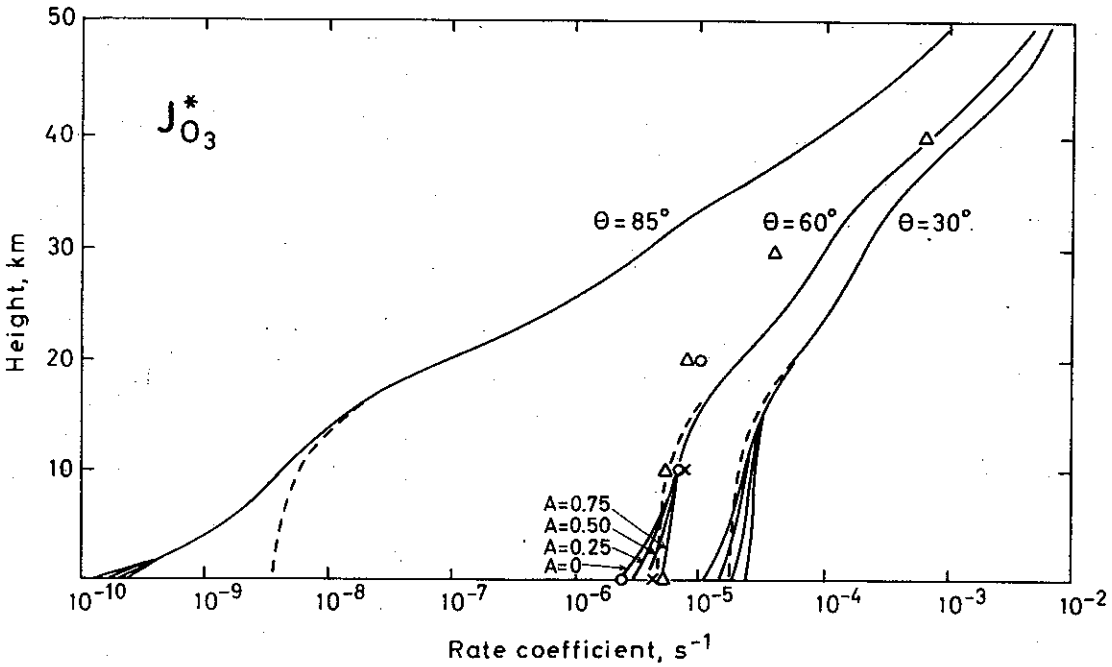

Fig. 4. Photodissociation coefficients of O_3 leading to the formation of excited state atomic oxygen ($O(^1D)$) through the reactions R1 and R2 (see Table 2) for different solar zenith angles θ in the case of absorption only, and in the case of multiple scattering with different surface albedos A. The dashed line gives coefficients in the case of pure absorption. The numbers denoted by Δ, O, and × give the photodissociation rate in the case of pure absorption, and in the cases of molecular scattering with the surface albedo equal to zero, and equal to 0.5, respectively, obtained by Luther & Gelinas (1976).

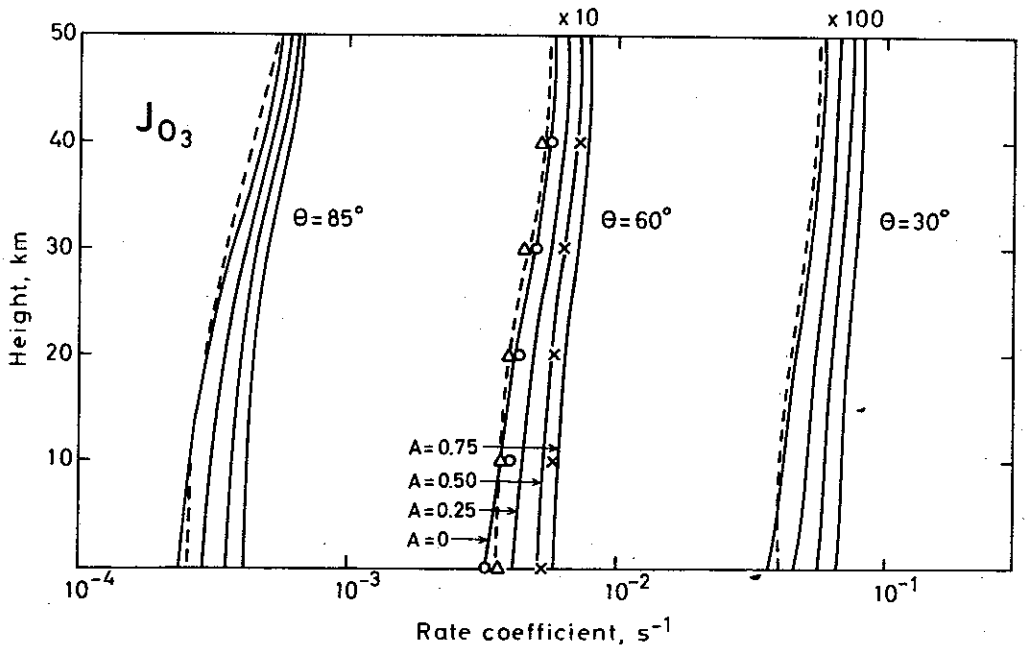

Fig. 5. Photodissociation coefficients of O_3 leading to the formation of ground state atomic oxygen ($O(^3P)$) through the reactions R2 and R3, for the same conditions as in Fig. 4. The numbers Δ, O, and × represent photodissociation rates similar to the rates in figure 4.

ciencies recommended in the CIAP monograph 4 (1975).

Dissociation of H_2O_2 is assumed to take place at wavelengths up to approximately 380 nm. The quantum efficiency above 280 nm is, however, rather uncertain. We have assumed that it decreases rapidly with increasing wavelength. This is a common assumption in stratospheric modelling (see for instance Nicolet 1975; Shimazaki & Whitten 1976). It should, however, be mentioned that Leighton (1961) used a quantum efficiency equal to one above 280 nm, leading to much

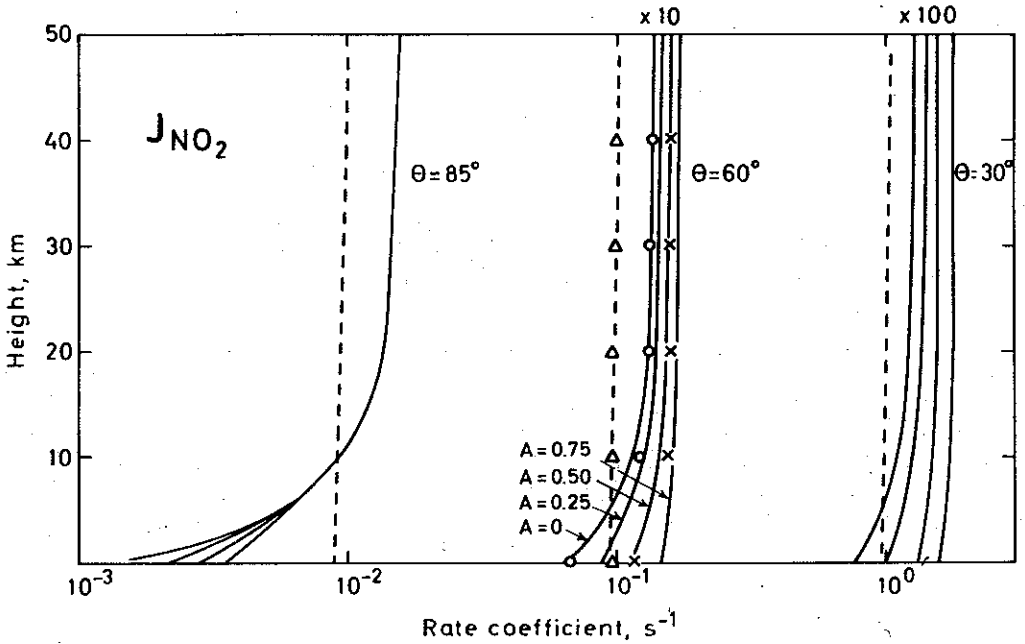

Fig. 6. Photodissociation coefficients of NO_2 (reaction R4) for the same conditions as in Fig. 4. The number Δ, O, and × represent photodissociation rates similar to the rates in Fig. 4.

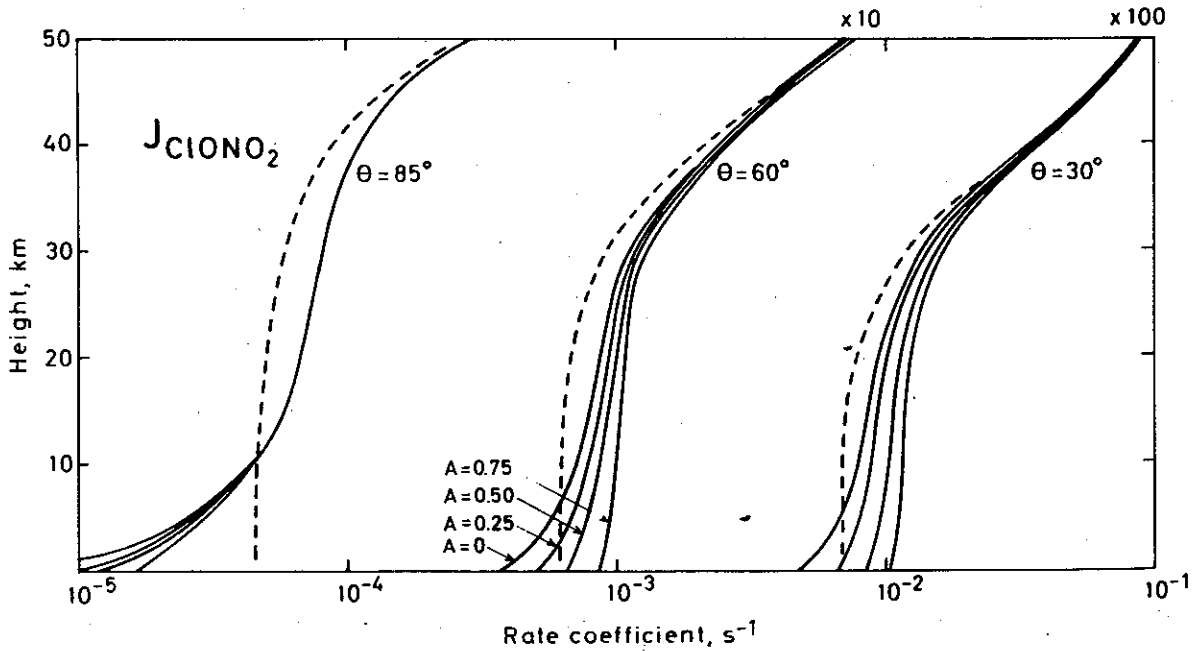

Fig. 7. Photodissociation coefficients of $ClONO_2$ (reactions R5) for the same conditions as in Fig. 4.

higher dissociation rates of H_2O_2, especially in the troposphere. For $\lambda < 280$ nm the values of H_2O_2 absorption, recommended in the CIAP Monograph 4 (1975), have been applied.

Absorption cross sections of O_3 (leading to the formation of $O(^3P)$) are taken from Ackerman (1971). In addition we have assumed that in the wavelength region 300 to 327 nm where α (the quantum efficiency for $O(^1D)$ formation) varies between 1 and 0, $O(^3P)$ is formed at a rate equal to $1-\alpha$.

Dissociation rates and dissociation products for the compounds HNO_2, HNO_3, N_2O_5, NO_3, and CH_2O are based on the recommendation in the

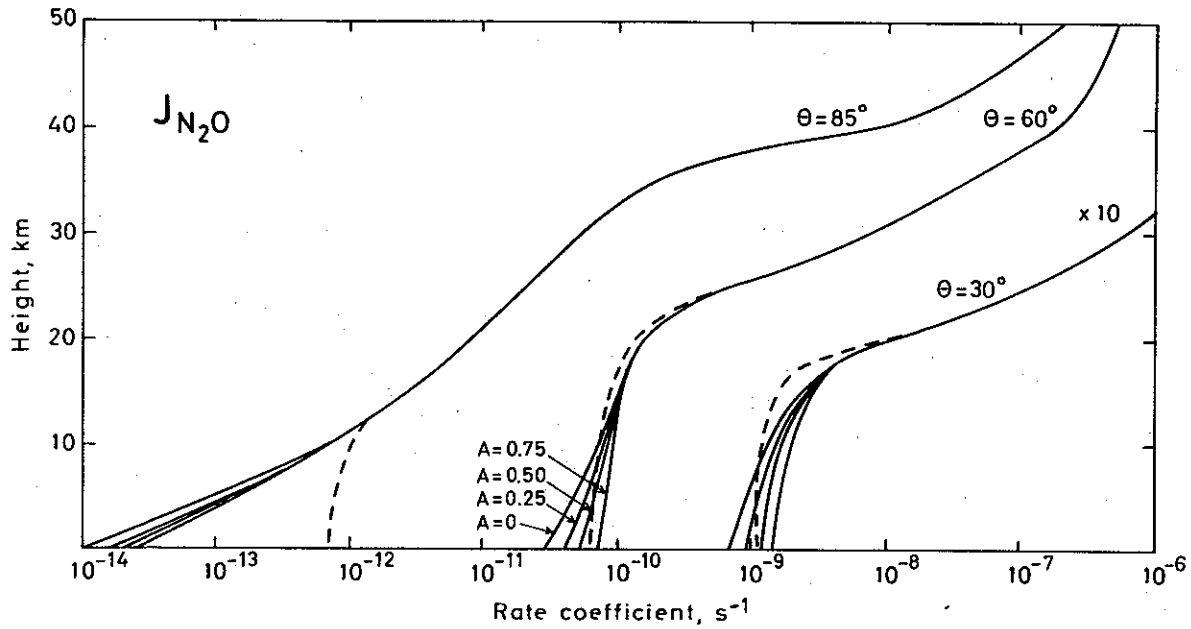

Fig. 8. Photodissociation coefficients of N_2O (reaction R6) for the same conditions as in Fig. 4.

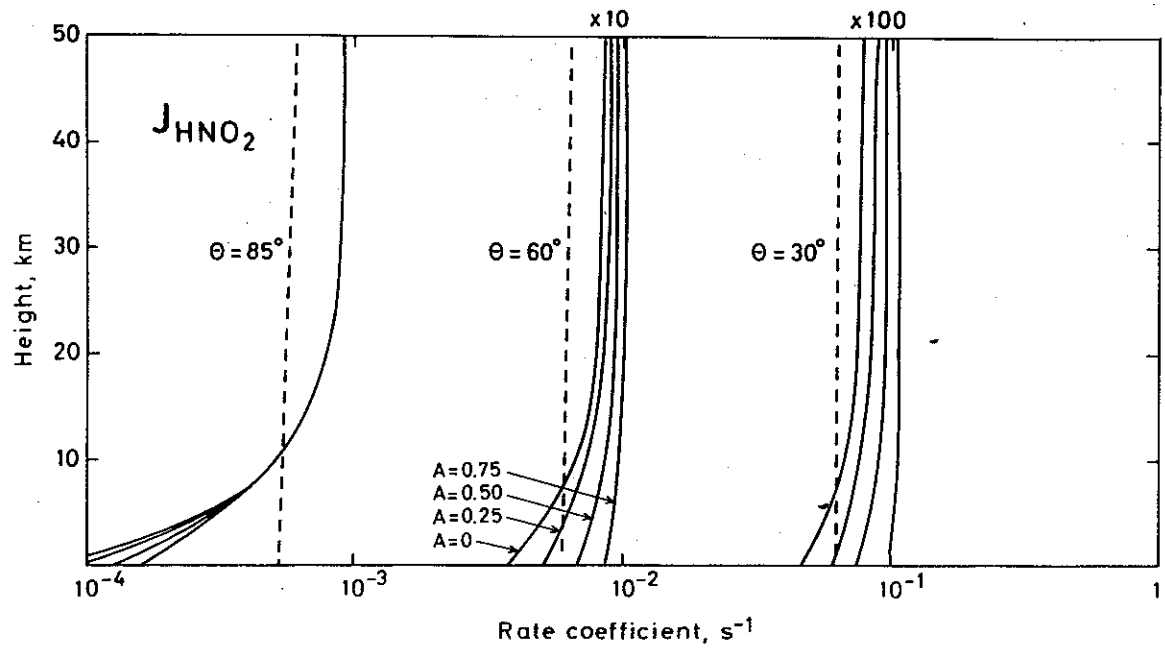

Fig. 9. Photodissociation coefficients of HNO_2 (reaction R7) for the same conditions as in Fig. 4.

CIAP Monograph 4 (1975) (see Table 2). Absorption cross sections of N_2O are corrected in accordance with the recent measurements of Johnston & Selwyn (1975), and the cross sections for $ClONO_2$ dissociation have been provided by Rowland (1976, private communications).

Calculated dissociation rates for the different species at the solar zenith angles 30°, 60°, and 85° are given in Figures 4–15.

The calculated dissociation rates of O_3 (J_{O_3} and $J^*_{O_3}$) and NO_2 of Luther & Gelinas (1976) given for a solar zenith angle of 60° are included in the figures of these species for comparison.

As discussed in the previous chapter, the effect

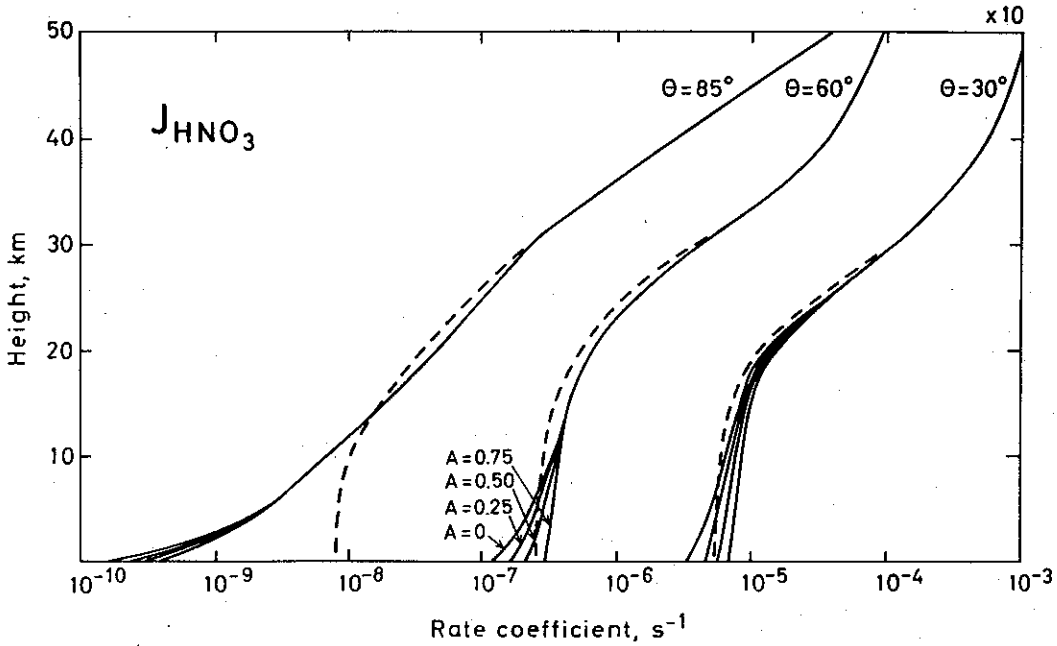

Fig. 10. Photodissociation coefficients of HNO_3 (reaction R8) for the same conditions as in Fig. 4.

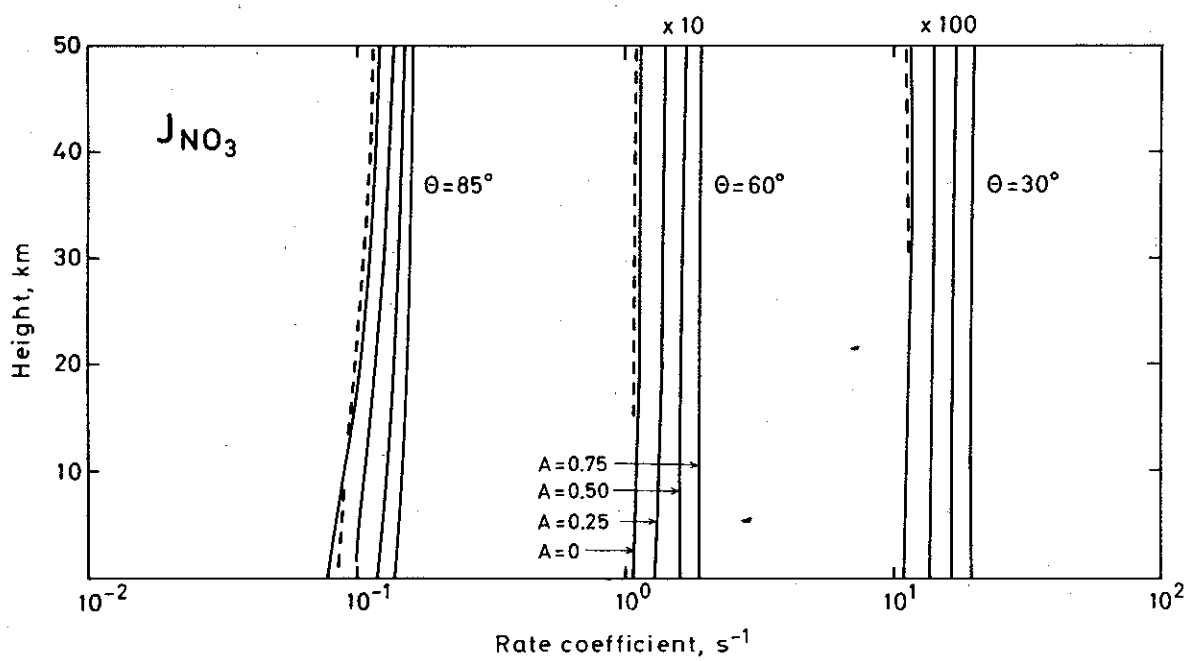

Fig. 11. Photodissociation coefficients of NO_3 (reaction R9) for the same conditions as in Fig. 4.

of molecular scattering and ground reflection varies markedly with wavelength, especially in the UV region. The contribution from these processes to the photodissociation rate will therefore depend strongly on the wavelength region where dissociation takes place.

Gases which are dissociated mainly at $\lambda < 300$ nm, where radiation is strongly absorbed by ozone, are affected little by scattering and reflection in the stratosphere. This is typical for gases like O_3 ($O(^1D)$ formation), HNO_3, N_2O, and H_2O_2. It is, however, interesting to notice that dissociation rates are markedly reduced by scattering at ground level. A large albedo, on the other hand, may com-

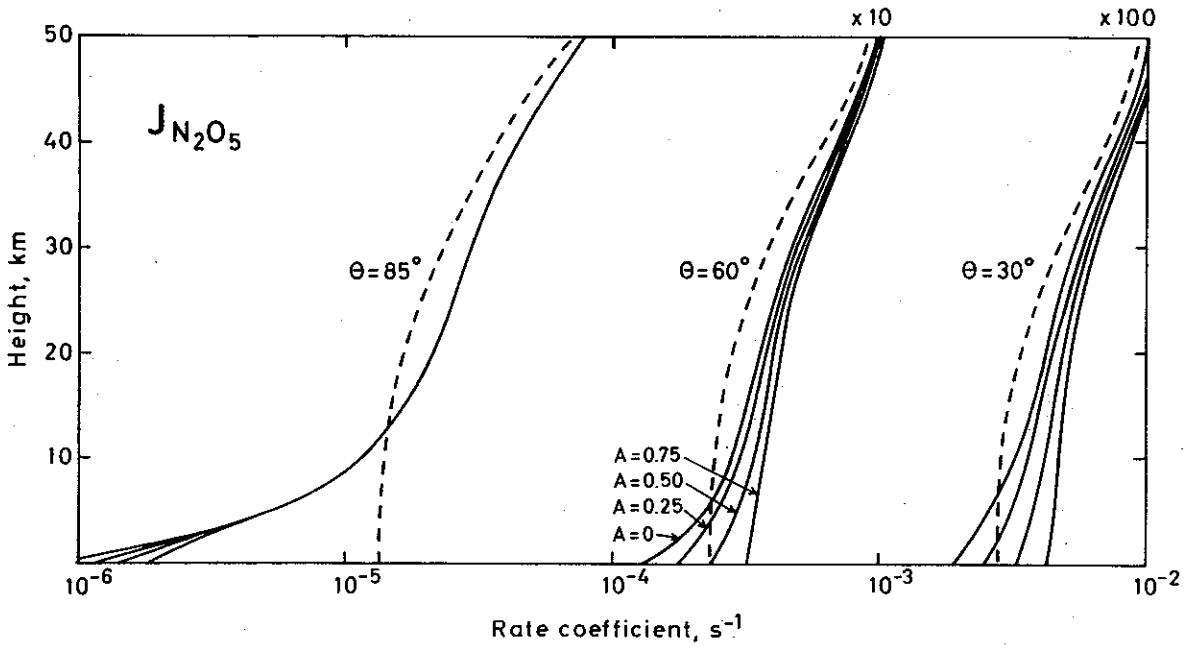

Fig. 12. Photodissociation coefficients of N_2O_5 (reaction R10) for the same conditions as in Fig. 4.

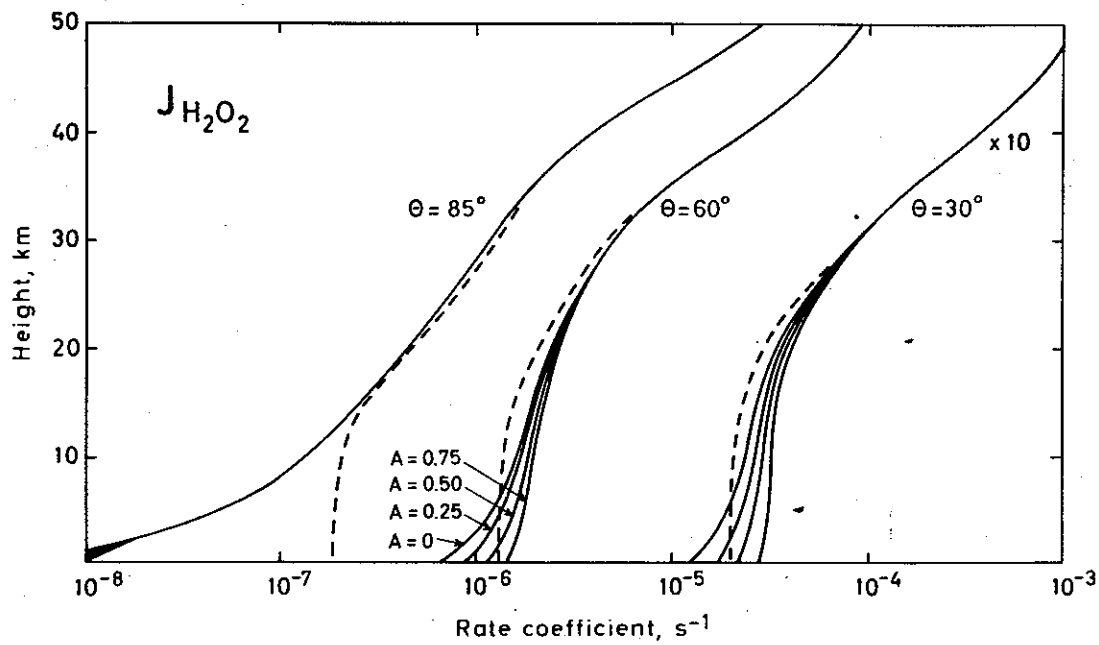

Fig. 13. Photodissociation coefficients of H_2O_2 (reaction R11) for the same conditions as in Fig. 4.

pensate for the effect of molecular scattering in the lower troposphere. An accurate determination of dissociation rates is especially important for the formation of $O(^1D)$ in the lower troposphere, since it is a key component in the chemistry of the background atmosphere. For gases like HNO_3 and N_2O, dissociation in the troposphere is too slow to make scattering or ground reflection important. Characteristic for the dissociation rates of these gases is the strong increase with height.

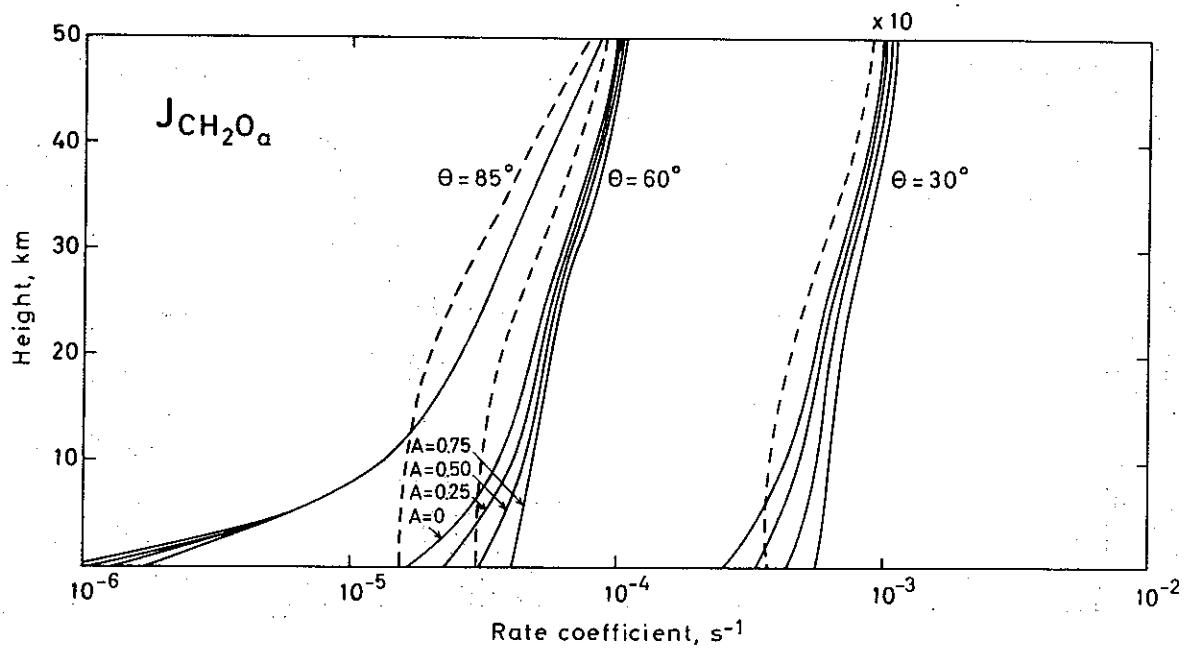

Fig. 14. Photodissociation coefficients of CH_2O leading to the formation of H and HCO (reaction R12) for the same conditions as in Fig. 4.

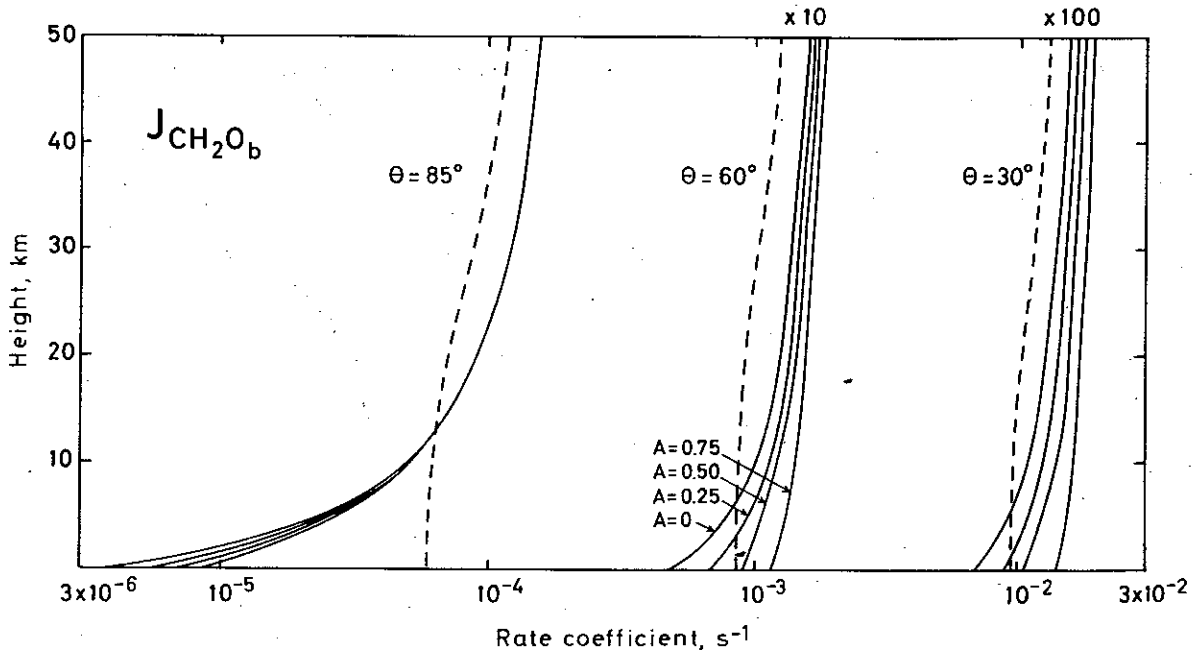

Fig. 15. Photodissociation coefficients of CH_2O leading to the formation of H_2 and CO (reaction R13) for the same conditions as in Fig. 4.

Other types of gases are dissociated in the UV region, but have a large part of their dissociation at wavelengths greater than 300 nm, e.g. CH_2O, N_2O_5, $ClONO_2$, NO_2, HNO_2. Molecular scattering will in these cases lead to marked increases in stratospheric fluxes, and to pronounced decrease in the fluxes reaching the ground. Ground reflection plays a significant role in the troposphere, but, except for the dissociation of NO_2 and HNO_2 which are affected little by ozone absorption, it becomes less pronounced in the stratosphere due to ozone absorption. It is further seen that the effect of ground reflection depends strongly on the solar zenith angle.

Finally we have the gases which have a strong photo-dissociation in the visible part of the solar spectrum. Typical examples are O_3 ($O(^3P)$ formation) and NO_3. Molecular scattering is found to have a small effect on dissociation rates of these species. The changes in photon fluxes are found to be dominated by ground reflection, provided the Earth's albedo is sufficiently high.

Comparisons are made with the calculated dissociation rates of O_3 and NO_2 obtained by Luther and Gelinas (1976) at a solar zenith angle of 60°, for the case of pure absorption only, the case of molecular scattering, and the case of molecular scattering and surface albedo ($A=0{\cdot}5$).

Our calculated profiles for J_{O_3} and J_{NO_2} are in good agreement with the results of Luther and Gelinas at most heights, in all three cases. As could be expected from the flux calculations, our model seems to underestimate the effect of molecular scattering around the tropopause heights (10–20 km). In the middle and upper stratosphere ($z>20$ km), and in the lower troposphere, however, the calculation of photon fluxes as a result of molecular scattering and ground reflection is in good agreement with the more accurate calculations; the discrepancy is within a few %. The calculated profiles of $J^*_{O_3}$ cannot be directly compared, since the dissociation is critically dependent on the ozone height distribution. The differences in the rates obtained in the two models at 20 and 30 km therefore reflect the different height profiles of ozone used. Luther and Gelinas have an ozone profiles with maximum densities at 25 km; in our model, maximum ozone densities are at 18 km. The result is that in our calculation the photon fluxes penetrate to lower heights before being absorbed by ozone. It is interesting to see that at ground level, where the total column densities of ozone differ little in the models, our calculations of the absolute rates of $J^*_{O_3}$, and of the relative rates due to molecular scattering and to ground reflection, are in very good agreement with the rates obtained by Luther and Gelinas. This is in agreement with what we found when comparing our results with the calculations of Sundararaman et al. (1975). The scattered fluxes reaching the Earth's surface at wavelengths greater than 300 nm agreed well, despite different height profiles, provided the total column density of ozone was the same.

4. CONCLUSIONS

With the use of the simplified method described in this paper, we are able to incorporate in time-dependent chemical models the calculations of the contribution from molecular scattering and ground reflection to the photodissociation rates of atmospheric gases. The importance of this method is illustrated by the good agreement with models where more accurate methods are used to solve the equation of radiative transfer. One result of these calculations is that for gases which are dissociated in the UV region, molecular scattering markedly reduces the photo-dissociation rates at ground level. This effect may, however, partly be compensated for by a large surface albedo. One rate of special importance is $J^*_{O_3}$ (reaction R1 in table 2), which determines the formation of hydroxyl radicals in the background atmosphere. It is approximately reduced to half its value at ground level when molecular scattering is included.

Another aspect of including molecular scattering and ground reflection in chemical models is that they may have large consequences for the stratospheric ozone depletion theory. The immediate effect is to increase the photodissociation rates of species like O_3, NO_2, and $ClONO_2$. To what extent this will affect the ozone chemistry, will be discussed in another paper.

REFERENCES

Ackerman, M. 1971. p. 149 in *Mesospheric Models and Related Experiments*. D. Reidel Publ. Company, Dordrecht, Holland.

CIAP Monograph 4. 1975. The Natural and Radiatively Perturbed Troposphere. Final Report.

Crutzen, P. J., Isaksen, I. S. A. & McAffe, J. 1976. *J. Geoph. Res.* (in press).

Hesstvedt, E. & Isaksen, I. S. A. 1974. Report No. 6, August 1974, Institutt for Geofysikk, Universitetet i Oslo.

Isaksen, I. S. A. & Crutzen, P. J. 1976. *Geophys. Norv. 31*, No. 4.

Johnston, H. S. 1973. CIAP Quarterly Progress Report, March–June 1973.

Johnston, H. S. & Selwyn, G. 1975. *Geophys. Res. Lett. 2*, 549–551.

Leighton, P. E. 1961. *Photochemistry of Air Pollution*. Academic Press, New York and London.

Lin, C. L. & De More, W. B. 1973. *Photochem. 2*, 161–164.

Luther, F. M. & Gelinas, R. J. 1976. *J. Geophys. Res. 81*, 1125–1132.

Moortgat, G. K. & Warneck, P. 1975. *Z. Naturforsch. 30a*, 835–844.

Nicolet, M. 1975. *Rev. Geophys. Space Phys. 13*, 593–636.

Sundararaman, N., St. John, D. E. & Venkateswaran, S. U. 1975 DOT-TST-75-101. US. Dep. Transportation.

Warneck, P. 1975. *Planet. Space Sci. 23*, 1507–1518.

Photochemistry of mixtures of hydrocarbons and nitrogen oxides in air

EIGIL HESSTVEDT, ØYSTEIN HOV & IVAR S. A. ISAKSEN
Institute of Geophysics, University of Oslo

Hesstvedt, E., Hov, Ø. & Isaksen, I. S. A. Photochemistry of mixtures of hydrocarbons and nitrogen oxides in air. *Geophysica Norvegica*, Vol. 31, No. 6, 1977.

A time-dependent photochemical model is used to analyse the chemical evolution in mixtures of air, nitrogen oxides, and four alternative hydrocarbons: ethylene, propylene, *n*-butane, and *n*-hexane. Time integrations are made for a four-hour period around noon, for different seasons, at 40° and 60° latitude. The formation of secondary pollutants such as ozone, hydrogen peroxide, formaldehyde, acetaldehyde, formic acid, nitrous acid, nitric acid, and peroxyacetyl nitrate (PAN) is found to depend strongly upon the hydrocarbon/nitrogen oxide ratio. When, for propylene as hydrocarbon, this ratio is below 1 or above 10^3, secondary pollutants are not formed. The production has a maximum when the ratio takes the value 3. The dependence on solar radiation is less pronounced than generally assumed; secondary pollutants form at approximately the same rate in spring, summer, and fall, and at 40° and 60° latitude. Only in winter, notably at 60° latitude, is oxidant formation significantly slowed down. We emphasize the importance of the radicals HO_2 and RO_2 for the formation of secondary pollutants.

E. Hesstvedt, Institute of Geophysics, University of Oslo, P.O. Box 1022, Blindern, Oslo, 3, Norway

1. INTRODUCTION

Air pollution in the form of hydrocarbons and nitrogen oxides may, under influence of ultraviolet sunlight, on special occasions lead to formation of gases, among others ozone, aldehydes, and PAN, which have undesirable effects on man and vegetation. Photochemical smog, i.e. situations when ozone and other pollutants exceed certain standards, became a serious problem in Los Angeles in the early 1940's. Today many big cities in different parts of the world with heavy automobile traffic struggle with the same problem. Emissions of hydrocarbons and nitrogen oxides from industry are also significant, and this will in many places add to the burden caused by automobiles.

The formation of smog has turned out to be a complex problem which may be conveniently studied in photochemical models. The purpose of such models is twofold: first, they shall give us the best possible insight into the main features of the chemical mechanism of smog formation. Second, they can be used to forecast smog events, either on a climatological scale or in a given situation. The purely photochemical model then has to be combined with a transport model with built-in sources of the basic pollutants. This, of course, sets certain limits on the number of reactions we can consider, and certain simplifications are necessary. There has, however, been a clear tendency to go too far in these simplifications, and this may have led to errors in the computations of oxidant formation. It is our opinion that a more comprehensive and realistic background chemistry does not represent an obstacle as far as computer time is concerned. We further find that only little is gained by using complex and time-consuming mathematical methods when computing the development of chemical components; with a time-step of, let us say, 10 seconds, the partial differential equations may be regarded as linear without significant loss of accuracy.

This paper was submitted to the Norwegian Academy of Science and Letters, 22 October 1976. The manuscript was presented 28 June 1976.

It is the aim of this paper to formulate models which describe the chemical development in air mixed with nitrogen oxides and different hydrocarbons: ethylene, propylene, *n*-butane, and *n*-hexane. These are typical combustion products from fossil fuels. Our paper should be regarded as an extension of a previous paper by one of the authors (Hesstvedt 1975) where only ethylene was considered. That paper emphasized the importance of the ratio hydrocarbons/nitrogen oxides (below denoted as HC/NO_x) for the formation of oxidants. The same ratio also governs the formation of other toxic components such as aldehydes and PAN. In the present paper we demonstrate the importance of the HC/NO_x ratio also when other hydrocarbons (propylene, *n*-butane, *n*- hexane) are considered. In these cases we base our photochemistry on a reaction scheme proposed by Demerjian et al. (1974).

Even for studies of a polluted atmosphere it is important to have a good representation of the reactions between inorganic compounds which take place in the 'clean' atmosphere. Recent years' intensified research in atmospheric chemistry in general has led to a substantial increase in knowledge about the kinetics of reactions in the background atmosphere. The laboratory work up to 1975 has crystallized in a comprehensive compilation of reaction rate coefficients (Garvin & Hampson 1975). The models we shall present here are based upon these recommended data.

2. PHOTODISSOCIATION

Solar radiation is the driving force in the chemistry of the 'clean' as well as the polluted atmosphere. Stratospheric ozone absorbs practically all solar radiation of wavelengths shorter than $\lambda = 285$ nm. Longer waves are attenuated to a degree which for a given wavelength depends primarily on ozone column density and solar zenith angle.

Photodissociation of ozone will produce excited atomic oxygen, $O(^1D)$, for waves shorter than $\lambda = 320$ nm. $O(^1D)$ reacts readily with water vapor whereby the radical HO is formed. HO and HO_2 are key components in atmospheric chemistry. In 'clean' air, the reaction $O(^1D) + H_2O \rightarrow HO + HO$ is the main source; when hydrocarbons are present, they will gradually oxidize, and with the passage of time take over as the main source of odd hydrogen. Results from theoretical models will obviously depend very much upon an accurate determination of the dissociation rate for O_3. This is also true for the contributions from wavelengths longer than $\lambda = 320$ nm. Similarly, the results will depend on how well we can determine the rate coefficient for photodissociation of NO_2. An error here would directly influence the computation of ozone. We also emphasize the importance of using the best possible values for other dissociation rate coefficients in modelling work.

Our computations of the solar fluxes at the Earth's surface are based upon flux data and absorption cross-sections for ozone, given by Ackerman (1971).

On its way through the atmosphere the solar radiation is depleted by absorption by atmospheric gases, by Rayleigh scattering, and by absorption and scattering of aerosols. However, the concentration, size distribution, and composition of aerosols vary so much in time and space that it is difficult to select a representative average condition. For this reason we have disregarded the effect of aerosols in our computations.

Apart from ozone, NO_2 is the only absorbing gas of importance for wavelengths of interest to surface air chemistry. Its abundance in the troposphere is not well known. However, on the basis of observations and theoretical models it has been suggested that NO_2 absorption amounts to about 1% in the background atmosphere (Hesstvedt & Isaksen 1974). In cases of air pollution the absorption may become considerably stronger; we have, however, disregarded this effect in our computations.

In the present work solar fluxes at ground level are obtained by considering ozone absorption and Rayleigh scattering. Reduction of the solar flux for a particular wavelength due to ozone absorption alone is obtained from Beer's law. The method we use to account for Rayleigh scattering is described in detail by Isaksen et al. (1976). The method involves a simplification: one half of the scattered light is assumed to proceed in the direction of the direct beam, the second half goes in the opposite direction. Multiple scattering up to

the fourth order is considered. Scattering of higher order is found to have negligible effect on the fluxes. The advantage of this method is that it greatly improves the accuracy in calculations of solar fluxes compared to pure absorption, without being too time-consuming. Solar fluxes obtained by this method are found to differ little from fluxes obtained from extensive models based on more elaborate calculations of the scattering.

The results of our computations of dissociation rate coefficients are given in Table 1. The data represent mean values for a four-hour period centered around local noon. Computations are made for two latitudes, 40° and 60°, and for four seasons: summer, fall, winter, and spring, in order to indicate the dependence on latitude and time of the year. Since the data for fall and spring equinoxes are nearly the same (the difference is due to different column densities of ozone), models are only computed for summer, winter and spring.

3. PHOTOCHEMISTRY OF THE BACKGROUND ATMOSPHERE

When photochemical smog is studied, one is primarily interested in the production of certain contaminants, such as ozone, hydrogen peroxide, aldehydes, and PAN. These species are, however, closely interrelated. When high levels of ozone are reached, the other species will be abundant as well. We will therefore focus our discussion on mechanisms which produce ozone and emphasize the significance of radical reactions involving HO, HO_2, NO, and NO_2. The reactions which are considered in our model are listed in Table 2.

Levy (1971) drew attention to the important role of the hydroxyl radical in tropospheric chemistry. He showed that the production of HO from the reaction

$$O(^1D)+H_2O \rightarrow 2HO \qquad \text{(R2.22)}$$

initiates formation of HO_2, CH_3, CH_3O, CH_3O_2, and HCO; all these radicals are important links in the complex chemistry of the unpolluted, as well as the polluted atmosphere. In a detailed analysis of radical reactions in the troposphere, Crutzen (1973) showed that HO and HO_2 may provide a production of ozone in the lower troposphere which exceeds the downward flux of ozone from the stratosphere calculated by Fabian & Junge (1970). Estimates of the combined effect of these sources on tropospheric ozone, based on chemical-diffusive models, are given by Hov (1975) and by Isaksen & Crutzen (1976).

The formation of HO and HO_2 in the troposphere is initiated by photolysis of ozone

$$O_3+h\nu \rightarrow O(^1D)+O_2 \quad \lambda<320\text{ nm} \qquad \text{(R7.h}\nu\text{ b)}$$

followed by reaction R2.22. Estimates of the production of hydroxyl depend critically upon the data for the quantum yield of $O(^1D)$ production. For wavelengths less than 310 nm, the efficiency

Table 1. Dissociation rate coefficients (s^{-1}), mean values for the period 10^h–14^h. For ozone, subscript '*a*' refers to $\lambda>320$ nm, subscript '*b*' to $\lambda<320$ nm. For HCHO, subscript '*a*' refers to CHO and H, while subscript '*b*' refers to CO and H_2 as daughter products. (The notation $x(-y)$ stands for $x \cdot 10^{-y}$.)

	40°				60°			
	Summer	Spring	Fall	Winter	Summer	Spring	Fall	Winter
$O_{3,a}$	3.7 (−4)	3.5 (−4)	3.6 (−4)	3.1 (−4)	3.5 (−4)	3.1 (−4)	3.2 (−4)	2.0 (−4)
$O_{3,b}$	1.7 (−5)	7.3 (−6)	1.2 (−5)	2.2 (−6)	8.4 (−6)	1.3 (−6)	2.8 (−6)	2.3 (−9)
H_2O_2	2.4 (−6)	1.9 (−6)	2.1 (−6)	1.3 (−6)	2.0 (−6)	1.2 (−6)	1.4 (−6)	1.5 (−7)
HNO_2	4.7 (−4)	4.4 (−4)	4.4 (−4)	3.7 (−4)	4.5 (−4)	3.8 (−4)	3.8 (−4)	1.2 (−4)
HNO_3	4.3 (−7)	2.7 (−7)	3.4 (−7)	1.3 (−7)	2.9 (−7)	1.0 (−7)	1.5 (−7)	1.6 (−9)
NO_2	8.0 (−3)	7.5 (−3)	7.5 (−3)	6.4 (−3)	7.6 (−3)	6.5 (−3)	6.5 (−3)	2.4 (−3)
N_2O_5	2.1 (−5)	1.8 (−5)	1.9 (−5)	1.3 (−5)	1.8 (−5)	1.2 (−5)	1.3 (−5)	1.9 (−6)
NO_3	8.9 (−2)	8.7 (−2)	8.8 (−2)	8.2 (−2)	8.8 (−2)	8.2 (−2)	8.3 (−2)	5.5 (−2)
$HCHO_a$	2.8 (−5)	2.3 (−5)	2.5 (−5)	1.6 (−5)	2.4 (−5)	1.6 (−5)	1.7 (−5)	2.0 (−6)
$HCHO_b$	7.0 (−5)	6.2 (−5)	6.4 (−5)	4.7 (−5)	6.4 (−5)	4.8 (−5)	5.0 (−5)	8.5 (−6)
CH_3CHO	2.0 (−5)	1.3 (−5)	1.6 (−5)	5.4 (−6)	1.5 (−5)	8.8 (−6)	7.5 (−6)	6.0 (−8)

is close to one (Hampson 1973, Lin & DeMore 1973), while data are controversial for longer wavelengths. Recent measurements indicate a gradual decrease in quantum yield above 310 nm, approaching zero around 320 nm (Johnston 1973). A certain temperature dependence may also exist (Moortgat & Warneck 1975).

The chain of reactions which transfers methane to carbon monoxide represents another possible source of HO and HO_2 (Levy 1971). Hydroxyl is consumed in the initial reaction

$$HO + CH_4 \rightarrow H_2O + CH_3 \qquad \text{(R19.56)}$$

However, the hydrogen atoms in the methyl ra-

Table 2*a*. Scheme for oxygen-hydrogen-nitrogen reactions considered in the model. Units: cm^6 molecule^{-2} s^{-1} for three-body reactions, cm^3 molecule^{-1} s^{-1} for two-body reactions, and s^{-1} for unimolecular reactions.

R1.4.M	$O + O_2 + M \rightarrow O_3 + M$	$1.1 \times 10^{-34} \exp(510/T)$
R1.10	$O + NO_2 \rightarrow O_2 + NO$	9.12×10^{-12}
R2.M	$O(^1D) + M \rightarrow O + M$	5.88×10^{-11}
R2.22	$O(^1D) + H_2O \rightarrow 2HO$	3.5×10^{-10}
R4.18.M	$O_2 + H + M \rightarrow HO_2 + M$	$2.1 \times 10^{-32} \exp(290/T)$
R7.hva	$O_3 + h\nu \rightarrow O + O_2$	$J_{O_3,a}$
R7.hvb	$O_3 + h\nu \rightarrow O(^1D) + O_2$	$J_{O_3,b}$
R7.9	$O_3 + NO \rightarrow O_2 + NO_2$	$9.0 \times 10^{-13} \exp(-1200/T)$
R7.10	$O_3 + NO_2 \rightarrow O_2 + NO_3$	$1.2 \times 10^{-13} \exp(-2450/T)$
R7.19	$O_3 + HO \rightarrow O_2 + HO_2$	$1.6 \times 10^{-12} \exp(-1000/T)$
R7.20	$O_3 + HO_2 \rightarrow 2O_2 + HO$	$1 \times 10^{-13} \exp(-1250/T)$
R9.11	$NO + NO_3 \rightarrow 2NO_2$	8.7×10^{-12}
R9.19	$NO + HO \rightarrow HNO_2$	5.6×10^{-12}
R9.20	$NO + HO_2 \rightarrow HO + NO_2$	1×10^{-12}
R10.hv	$NO_2 + h\nu \rightarrow O + NO$	J_{NO_2}
R10.11a	$NO_2 + NO_3 \rightarrow O_2 + NO + NO_2$	$2.3 \times 10^{-13} \exp(-1000/T)$
R10.11b	$NO_2 + NO_3 \rightarrow N_2O_5$	3.8×10^{-12}
R10.19	$NO_2 + HO \rightarrow HNO_3$	1×10^{-11}
R10.20	$NO_2 + HO_2 \rightarrow O_2 + HNO_2$	3×10^{-14}
R11.hv	$NO_3 + h\nu \rightarrow NO_2 + O$	J_{NO_3}
R14.hv	$N_2O_5 + h\nu \rightarrow NO_2 + NO_3$	$J_{N_2O_5}$
R14	$N_2O_5 \rightarrow NO_2 + NO_3$	$5.7 \times 10^{14} \exp(-10600/T)$
R19.20	$HO + HO_2 \rightarrow O_2 + H_2O$	2×10^{-11}
R19.23	$HO + H_2O_2 \rightarrow HO_2 + H_2O$	$1.7 \times 10^{-11} \exp(-910/T)$
R19.25	$HO + HNO_2 \rightarrow NO_2 + H_2O$	6.8×10^{-12}
R19.26	$HO + HNO_3 \rightarrow NO_3 + H_2O$	1.3×10^{-13}
R20.20	$HO_2 + HO_2 \rightarrow O_2 + H_2O_2$	2×10^{-11}
R23.hv	$H_2O_2 + h\nu \rightarrow 2HO$	$J_{H_2O_2}$
R25.hv	$HNO_2 + h\nu \rightarrow NO + HO$	J_{HNO_2}
R26.hv	$HNO_3 + h\nu \rightarrow NO_2 + HO$	J_{HNO_3}
R19.56	$HO + CH_4 \rightarrow H_2O + CH_3$	$2.36 \times 10^{-12} \exp(-1710/T)$

Table 2*b*. Methane oxidation scheme (same units as in Table 2*a*).

R4.49	$O_2 + CH_3 \rightarrow CH_3O_2$	5.1×10^{-13}
R9.51	$NO + CH_3O_2 \rightarrow NO_2 + CH_3O$	$3.3 \times 10^{-12} \exp(-500/T)$
R20.51	$HO_2 + CH_3O_2 \rightarrow O_2 + CH_3O_2H$	6.7×10^{-14}
R51.51	$CH_3O_2 + CH_3O_2 \rightarrow CH_3O_2H + \dot{C}H_2\dot{O}_2$	6.8×10^{-14}
R4.50	$O_2 + CH_3O \rightarrow HO_2 + HCHO$	3×10^{-18}
R52.hv	$CH_3O_2H + h\nu \rightarrow HO + CH_3O$	$J_{CH_3O_2H}$
R48.hva	$HCHO + h\nu \rightarrow H + CHO$	J_{HCHOa}
R48.hvb	$HCHO + h\nu \rightarrow H_2 + CO$	J_{HCHOb}
R19.48	$HO + HCHO \rightarrow H_2O + CHO$	1.4×10^{-11}
R4.47	$O_2 + CHO \rightarrow HO_2 + CO$	5.7×10^{-12}
R19.45	$HO + CO \rightarrow H + CO_2$	1.4×10^{-13}

dical may yield odd hydrogen molecules through further decomposition and thereby turn the methane oxidation chain into a net source of odd hydrogen. This decomposition can proceed along different paths (Hampson & Garvin 1975), and the production rates depend on which one is followed.

In the troposphere HO and HO_2 radicals are partly lost through the reaction

$$HO + HO_2 \rightarrow H_2O + O_2 \qquad (R19.20)$$

In the lower troposphere an even more important removal of HO and HO_2 comes from the reactions

$$HO_2 + HO_2 \rightarrow H_2O_2 + O_2 \qquad (R20.20)$$

$$NO_2 + HO \rightarrow HNO_3 \qquad (R10.19)$$

followed by heterogeneous removal of hydrogen peroxide and nitric acid. If we assume that these heterogeneous removals occur on a time scale of about ten days (Chameides 1975, Isaksen & Crutzen 1976), the removal of nitric acid by precipitation processes exceeds the gas phase decomposition through R26.hν, while the time scales are of the same order for hydrogen peroxide (see Table 1), and probably also for methylhydroperoxide. Heterogeneous reactions are therefore important in the background atmosphere since they control the content of odd hydrogen. However, in studies of phenomena on a time scale of less than one day, as we discuss here, heterogeneous reactions may be disregarded.

The formation of nitrous acid through the reaction

$$NO_2 + HO_2 \rightarrow HNO_2 + O_2 \qquad (R10.20)$$

can be disregarded as a sink for odd hydrogen, because HNO_2 is rapidly decomposed by photodissociation and odd hydrogen is reformed.

The significance of hydrogen peroxide and nitrous acid in a polluted atmosphere will be discussed later. It should be mentioned here that these two species are not broken down at night; they may therefore act as important sources of odd hydrogen at sunrise.

The chemistry of odd hydrogen in the troposphere involves a large number of reactions. It is a characteristic of the background atmosphere that the internal exchange processes between H, HO, and HO_2 proceed more rapidly than the loss reactions mentioned above. In the 'clean', as well as in the polluted atmosphere, ozone chemistry is closely linked to these cyclic hydrogen reactions. In a discussion of ozone chemistry it is essential to have the following reaction paths in mind:

Hydroxyl, which in the background atmosphere is formed by reaction R2.22, is mainly broken down and converted to HO_2 through the reactions

$$HO + CO \rightarrow H + CO_2 \qquad (R19.45)$$

$$O_2 + H + M \rightarrow HO_2 + M \qquad (R4.18.M)$$

In addition there is a substantial conversion of HO to HO_2 through the methane oxidation (R19.56) leading to the formation of formaldehyde:

$$O_2 + CH_3O \rightarrow HO_2 + HCHO \qquad (R4.50)$$

A description of the decomposition of formaldehyde will be given in connection with the discussion of the oxidation products from ethylene.

HO_2 plays an important role in the formation of ozone since it converts NO to NO_2

$$NO + HO_2 \rightarrow NO_2 + HO \qquad (R9.20)$$

Once NO_2 is formed, it is rapidly photodissociated

$$NO_2 + h\nu \rightarrow NO + O \qquad (R10.h\nu)$$

leading to ozone formation through reaction R1.4.M. Note that NO is converted to NO_2 without consumption of odd oxygen. It should be emphasized that the rapid conversion of NO to NO_2 through

$$O_3 + NO \rightarrow NO_2 + O_2 \qquad (R7.9)$$

is counteracted by the equally fast reactions R10.hν and R1.4.M. The net effect of these three reactions is zero.

An additional transfer of NO to NO_2 without consumption of odd oxygen occurs in the chain of reactions initiated by the oxidation of methane

$$NO + CH_3O_2 \rightarrow NO_2 + CH_3O \qquad (R9.51)$$

It will be shown below that similar reactions are significant for ozone formation when, in a polluted atmosphere, higher hydrocarbons are oxidized. In

such cases the production of HO_2 is intensified so that the rate of NO to NO_2 conversion through reaction R9.20 is also considerably accelerated.

In addition to its ozone producing effect, as already mentioned, HO_2 will also attack ozone directly through the reaction

$$O_3 + HO_2 \rightarrow HO + 2O_2 \qquad \text{(R7.20)}$$

In the background atmosphere these two effects are comparable; the net result will depend upon the ratio $[NO]/[O_3]$. An increase in this ratio, as is common in cases of pollution, favors the production of ozone.

A less important conversion of HO to HO_2 takes place through the reaction

$$O_3 + HO \rightarrow HO_2 + O_2 \qquad \text{(R7.19)}$$

Recycling of HO_2 to HO will take place through reactions R7.20 or R9.20. Reaction R7.19 will therefore always represent a net destruction of ozone.

Finally it should be mentioned that a destruction of ozone takes place because part of the nitrogen dioxide formed by reaction R7.9 goes to nitric and nitrous acid. Nitric acid is removed by precipitation, while nitrous acid is photodissociated and gives back nitric oxide (reaction R25.hν).

4. PHOTOCHEMISTRY OF THE POLLUTED ATMOSPHERE

In this section we shall discuss the chemical reactions which take place when air is polluted with nitrogen oxides (NO and NO_2, together called NO_x), and four different hydrocarbons: ethylene, propylene, *n*-butane, and *n*-hexane. For each hydrocarbon we define a photochemical model, and for each model several alternative models are computed where the mixing ratios of nitrogen oxides and hydrocarbons are varied within wide limits.

The large number of reactions which take place, and intermediate products which are formed (Demerjian et al. 1974), make it inconvenient to incorporate a complete chemistry of hydrocarbon oxidation products in our models. Since, however, most of the intermediate products turn out to have very short lifetimes (seconds or less), photochemical equilibrium is a good approximation. This means that transitions through intermediate components take place without time delay, and the more long-lived products may be considered as direct products. This makes it possible to reduce drastically the number of reactions and disintegration products without loss of accuracy or generality.

The densities of the more long-lived products must be computed in order to get an adequate picture of the time evolvement of the mixture, and also because some of them may have inherent toxicity (ozone, aldehydes, PAN, nitrogen dioxide, hydrogen peroxide).

Ethylene oxidation

Decomposition of ethylene is mainly due to reaction with hydroxyl

$$HO + C_2H_4 \rightarrow HCHO + CH_3 \qquad \text{(R19.57a)}$$

Less important are losses through reactions with atomic oxygen and ozone

$$O + C_2H_4 \rightarrow CH_3 + CHO \qquad \text{(R1.57a)}$$

$$O_3 + C_2H_4 \rightarrow HCHO + \dot{C}H_2\dot{O}_2 \qquad \text{(R7.57a)}$$

Formyl (CHO) reacts rapidly with molecular oxygen, whereby HO_2 is formed

$$O_2 + CHO \rightarrow CO + HO_2 \qquad \text{(R4.47)}$$

Decomposition of $\dot{C}H_2\dot{O}_2$ leads to production of odd hydrogen through a sequence of reactions ending with

$$O_2 + CH_2\dot{O}\dot{O} \rightarrow HO_2 + HCO_2 \qquad \text{(R4.57d)}$$

$$HCO_2 \rightarrow H + CO_2 \qquad \text{(R57e)}$$

As previously discussed, the oxidation of the methyl radical leads to conversion of NO to NO_2 (R9.51) and to the formation of HO_2 (R4.50).

Formaldehyde has a lifetime of some hours and is therefore included in our computational scheme. It is usually considered to be one of the main pollutants formed when hydrocarbons are oxidized. In fact we find it to be an important aldehyde in all the models we consider. Its decomposition yields odd hydrogen through the reaction

$$HCHO + h\nu \rightarrow H + CHO \qquad \text{(R48.h}\nu\text{a)}$$

which rapidly leads to the production of two HO_2 molecules through reactions R4.18M and R4.47. It also contributes to the conversion of HO to HO_2 through the reaction

$$HO + HCHO \rightarrow H_2O + CHO \quad \text{(R19.48)}$$

followed by reaction R4.47.

We should also notice that the above reactions, in addition to reaction

$$HCHO + h\nu \rightarrow H_2 + CO\,, \quad \text{(R48.h}\nu\text{b)}$$

act as an important source of carbon monoxide both in unpolluted and in polluted air.

Our computation of the products of ethylene decomposition is based on reactions listed in Table 3, in combination with reactions listed in Tables 2*a* and 2*b*.

Propylene oxidation

The complexity of the chemical scheme increases as we proceed to higher hydrocarbons. Similar to ethylene, the initial loss of propylene takes place mainly through reaction with hydroxyl, but reactions with ozone and atomic oxygen will also contribute:

$$HO + C_3H_6 \rightarrow H_2O + CH_2{=}C\dot{H}CH_2 \quad \text{(R19.59aI)}$$

$$HO + C_3H_6 \rightarrow CH_3\dot{C}HCH_2OH \quad \text{(R19.59aII)}$$

$$O_3 + C_3H_6 \rightarrow CH_3\overline{\dot{C}HCH_2OOO} \quad \text{(R7.59a)}$$

$$O + C_3H_6 \rightarrow \dot{C}_3H_6\dot{O} \quad \text{(R1.59a)}$$

Propylene may also be broken down through reaction with radicals such as HO_2, CH_3O, and CH_3O_2. We have tested the importance of these reactions in our model calculations, and find that they only contribute to the formation of pollutants in cases of extremely high propylene mixing ratio (> 10 ppm). Since such concentrations are of little practical significance, these reactions are omitted in the further discussion. We shall not make a complete discussion of all intermediate compounds, but emphasize reactions which are important for the key compounds in the systems.

In the chain of reactions following reaction R19.59aI, conversion of NO to NO_2 takes place through reaction

$$NO + \overline{CH_2CH(\dot{O}_2)CH_2O\dot{O}}$$

$$\rightarrow NO_2 + \overline{\dot{C}H_2CH(\dot{O})CH_2O\dot{O}} \quad \text{(R9.59f)}$$

Formaldehyde is formed in the subsequent reactions

$$\overline{\dot{C}H_2CH(\dot{O})CH_2O\dot{O}} \rightarrow HCHO + CH_2(\dot{O})CHO \quad \text{(R59g)}$$

$$CH_2(\dot{O})CHO \rightarrow CHO + HCHO \quad \text{(R59h)}$$

Formyl is converted to HO_2 through reaction R4.47.

In the chain of reactions following reaction R19.59aII, NO is converted to NO_2 through the reaction

$$NO + CH_3CH(\dot{O}_2)CH_2OH$$

$$\rightarrow NO_2 + CH_3CH(\dot{O})CH_2OH \quad \text{(R9.59j)}$$

and acetaldehyde is formed through the reaction

$$CH_3CH(\dot{O})CH_2OH \rightarrow CH_3CHO + \dot{C}H_2OH \quad \text{(R59k)}$$

Table 3. Ethylene oxidation scheme (same units as in Table 2*a*).

R19.57a	$HO + C_2H_4 \rightarrow HCHO + CH_3$	3×10^{-12}
R7.57a	$O_3 + C_2H_4 \rightarrow HCHO + \dot{C}H_2\dot{O}_2$	$9.0 \times 10^{-15} \exp(-2560/T)$
R1.57a	$O + C_2H_4 \rightarrow CH_3 + CHO$	$5.5 \times 10^{-12} \exp(-565/T)$
R4.57b	$O_2 + \dot{C}H_2\dot{O}_2 \rightarrow CH_2(\dot{O}_2)\dot{O}_2$	6.2×10^{-12}
R57c	$CH_2(\dot{O}_2)\dot{O}_2 \rightarrow O_2 + CH_2(\dot{O})\dot{O}$	$\geq 4.7 \times 10^{3}$
R4.57d	$O_2 + CH_2(\dot{O})\dot{O} \rightarrow HO_2 + HCO_2$	4.0×10^{-16}
R9.57d	$NO + CH_2(\dot{O})\dot{O} \rightarrow NO_2 + HCHO$	3.0×10^{-12}
R57e	$HCO_2 \rightarrow H + CO_2$	2.5×10^{8}

Acetaldehyde has a lifetime of some hours. It may become a main pollutant when propylene and higher hydrocarbons are oxidized. It is decomposed by photodissociation and by reaction with HO:

$$CH_3CHO + h\nu \rightarrow CHO + CH_3 \quad \text{(R59o.hν)}$$

$$HO + CH_3CHO \rightarrow H_2O + CH_3CO \quad \text{(R19.59o)}$$

Methyl and formyl radicals react with O_2 and form CH_3O_2, CO, and HO_2.

Formation of acetyl (CH_3CO) through reaction R19.59o is of special interest because it leads to the formation of peroxyacetyl nitrate (PAN) through this sequence of reactions:

$$O_2 + CH_3CO \rightarrow CH_3COO_2 \quad \text{(R4.59p)}$$

$$NO_2 + CH_3COO_2 \rightarrow CH_3COO_2NO_2 \text{ (PAN)} \quad \text{(R10.59q)}$$

The latter reaction competes with

$$NO + CH_3COO_2 \rightarrow NO_2 + CH_3CO_2 \quad \text{(R9.59q)}$$

which converts NO to NO_2, and which also represents an additional source of odd hydrogen and NO_2 by further oxidation (compare Table 4).

Table 4. Propylene oxidation scheme (same units as in Table 2*a*).

R19.59aI	$HO + CH_3CH{=}CH_2 \rightarrow H_2O + CH_2{=}C\dot{H}CH_2$	9.3×10^{-12}
R19.59aII	$HO + CH_3CH{=}CH_2 \rightarrow CH_3\dot{C}HCH_2OH$	6.0×10^{-12}
R7.59a	$O_3 + CH_3CH{=}CH_2 \rightarrow CH_3\overline{\dot{C}HCH_2OOO}$	$6.1 \times 10^{-15} \exp(-1900/T)$
R1.59a	$O + CH_3CH{=}CH_2 \rightarrow \dot{C}_3H_6\dot{O}$	$4.1 \times 10^{-12} \exp(-38/T)$
R4.59b	$O_2 + CH_2{=}C\dot{H}CH_2 \rightarrow CH_2{=}CHCH_2\dot{O}_2$	6.2×10^{-14}
R59c	$CH_2{=}CHCH_2\dot{O}_2 \rightarrow \overline{\dot{C}H_2CHCH_2O\dot{O}}$	2.7×10^{3}
R4.59e	$O_2 + \overline{\dot{C}H_2CHCH_2O\dot{O}} \rightarrow \overline{\dot{C}H_2CH(O_2)CH_2O\dot{O}}$	6.2×10^{-12}
R9.59f	$NO + \overline{\dot{C}H_2CH(\dot{O}_2)CH_2O\dot{O}} \rightarrow NO_2 + \overline{\dot{C}H_2CH(\dot{O})CH_2O\dot{O}}$	2.9×10^{-13}
R59g	$\overline{\dot{C}H_2CH(\dot{O})CH_2O\dot{O}} \rightarrow HCHO + CH_2(\dot{O})CHO$	6.8×10^{8}
R59h	$CH_2(\dot{O})CHO \rightarrow CHO + HCHO$	7.2×10^{8}
R4.59i	$O_2 + CH_3\dot{C}HCH_2OH \rightarrow CH_3CH(\dot{O}_2)CH_2OH$	6.2×10^{-12}
R9.59j	$NO + CH_3CH(\dot{O}_2)CH_2OH \rightarrow NO_2 + CH_3CH(\dot{O})CH_2OH$	2.9×10^{-13}
R59k	$CH_3CH(\dot{O})CH_2OH \rightarrow CH_3CHO + \dot{C}H_2OH$	2.5×10^{3}
R4.59l	$O_2 + \dot{C}H_2OH \rightarrow CH_2(\dot{O}_2)OH$	6.2×10^{-12}
R9.59m	$NO + CH_2(\dot{O}_2)OH \rightarrow NO_2 + CH_2(\dot{O})OH$	3.0×10^{-12}
R4.59n	$O_2 + CH_2(\dot{O})OH \rightarrow HO_2 + HCOOH$	2.4×10^{-15}
R59o.hν	$CH_3CHO + h\nu \rightarrow CHO + CH_3$	J_{CH_3CHO}
R19.59o	$HO + CH_3CHO \rightarrow H_2O + CH_3CO$	1.4×10^{-11}
R4.59p	$O_2 + CH_3CO \rightarrow CH_3COO_2$	6.2×10^{-11}
R9.59q	$NO + CH_3COO_2 \rightarrow NO_2 + CH_3CO_2$	2.9×10^{-13}
R10.59q	$NO_2 + CH_3COO_2 \rightarrow CH_3COO_2NO_2$ (PAN)	3.0×10^{-13}
R59r	$CH_3CO_2 \rightarrow CH_3 + CO_2$	2.2×10^{10}
R9.59s	$NO + CH_3COO_2NO_2 \rightarrow NO_2 + CH_3COO_2NO$	9.9×10^{-17}
R59tI	$CH_3\overline{\dot{C}HCH_2OOO} \rightarrow CH_3CH(\dot{O})CH_2\dot{O}_2$	4.7×10^{3}
R59tII	$\rightarrow CH_3CH(\dot{O}_2)CH_2\dot{O}$	4.7×10^{3}
R59u	$CH_3CH(\dot{O})CH_2\dot{O}_2 \rightarrow \dot{C}H_2\dot{O}_2 + CH_3CHO$	3.2×10^{3}
R59v	$CH_3CH(\dot{O}_2)CH_2\dot{O} \rightarrow HCHO + CH_3\dot{C}HO_2$	3.2×10^{3}
R4.59w	$O_2 + CH_3\dot{C}HO_2 \rightarrow CH_3CH(\dot{O}_2)\dot{O}_2$	6.2×10^{-12}
R59x	$CH_3CH(\dot{O}_2)\dot{O}_2 \rightarrow O_2 + CH_3CH(\dot{O})\dot{O}$	$\geq 4.7 \times 10^{3}$
R4.59y	$O_2 + CH_3CH(\dot{O})\dot{O} \rightarrow HO_2 + CH_3CO_2$	4.0×10^{-16}
R4.59zI	$O_2 + \dot{C}_3H_6\dot{O} \rightarrow CH_3CH(\dot{O})CH_2\dot{O}_2$	6.2×10^{-12}
R4.59zII	$\rightarrow CH_3CH(\dot{O}_2)CH_2\dot{O}$	6.2×10^{-12}

Since the two reactions are believed to proceed at almost the same rate, the formation of PAN depends critically on the ratio $[NO_2]/[NO]$. When this ratio exceeds unity, the loss of acetaldehyde through reaction R19.59o favors the formation of PAN. This is the case in smog situations.

The formation of PAN is proportional to the ratio

$$x_o = \frac{k_{10\cdot 59q}[NO_2]}{k_{10\cdot 59q}[NO_2] + k_{9\cdot 59q}[NO]} \quad (1)$$

The rate of the conversion of NO to NO_2 is proportional to

$$y_o = 1 - x_o \quad (2)$$

The formation of PAN through the reaction R10.59q may represent an important sink for nitrogen dioxide.

The reaction of ozone with propylene leads to the formation of acetaldehyde and formaldehyde with production rates equal to one half of the loss rate of propylene through the reaction R7.59a:

$$CH_3CH(\dot{O})CH_2\dot{O}_2 \rightarrow \dot{C}H_2\dot{O}_2 + CH_3CHO \quad (R59u)$$

$$CH_3CH(\dot{O}_2)CH_2\dot{O} \rightarrow HCHO + CH_3\dot{C}H\dot{O}_2 \quad (R59v)$$

As discussed previously, the decomposition of $\dot{C}H_2\dot{O}_2$ leads to the production of odd hydrogen through reactions R4.57d and R57e. Odd hydrogen is produced and methyl radicals formed from the decomposition of $CH_3\dot{C}H\dot{O}_2$ through the reactions

$$O_2 + CH_3CH(\dot{O})\dot{O} \rightarrow HO_2 + CH_3C\dot{O}_2 \quad (R4.59y)$$

$$CH_3C\dot{O}_2 \rightarrow CH_3 + CO_2 \quad (R59r)$$

In this reaction scheme we have omitted all reaction paths of minor importance (less than 5% of the main paths).

Reaction of propylene with atomic oxygen leads to the same products as through the reaction with ozone, after the following step:

$$O_2 + \dot{C}_3H_6\dot{O} \rightarrow CH_3CH(\dot{O})CH_2\dot{O}_2 \quad (R4.59zI)$$

$$\rightarrow CH_3CH(\dot{O}_2)CH_2\dot{O} \quad (R4.59zII)$$

The set of reactions which describes the decomposition of propylene, is listed in Table 4.

n-butane oxidation

Paraffins, C_nH_{2n+2}, are broken up more slowly than olefins, C_nH_{2n}, for any number n. Lower paraffins, e.g. methane, ethane, and propane, react too slowly to contribute to the formation of smog products on the time scale considered here. We shall therefore only consider higher paraffins (n-butane and n-hexane), which are emitted in considerable amounts in industrial regions and areas with heavy traffic, and which react on a time scale comparable to that of the lower olefins (ethylene).

For the paraffins, loss through reactions with ozone and atomic oxygen is assumed to be negligible compared to the loss through the reactions with hydroxyl.

The initial loss reaction for n-butane gives two separate shortlived products, each starting different reaction paths:

$$HO + nC_4H_{10} \rightarrow H_2O + \text{sec } C_4H_9 \quad (R19.60aI)$$

$$HO + nC_4H_{10} \rightarrow H_2O + nC_4H_9 \quad (R19.60aII)$$

(We have introduced the notations (Demerjian et al. 1974) sec C_4H_9 for $CH_3\dot{C}HCH_2CH_3$, nC_4H_9 for $CH_3CH_2CH_2\dot{C}H_2$). As previously we only discuss the reactions which influence the key components.

Conversion of NO to NO_2 takes place through the reaction

$$NO + \text{sec } C_4H_9\dot{O}_2 \rightarrow NO_2 + \text{sec } C_4H_9\dot{O} \quad (R9.60c)$$

Further decomposition of sec $C_4H_9\dot{O}$ proceeds through two equally important paths:

$$O_2 + \text{sec } C_4H_9\dot{O} \rightarrow HO_2 + CH_3COC_2H_5 \quad (R4.60d)$$

$$\text{sec } C_4H_9\dot{O} \rightarrow CH_3CHO + C_2H_5 \quad (R60d)$$

We do not compute the density of the shortlived intermediate sec $C_4H_9\dot{O}$, and derive the relative importance x_1 of R4.60d and y_1 of R60d from the expressions

$$x_1 = \frac{k_{4\cdot 60d}\cdot[O_2]}{k_{4\cdot 60d}\cdot[O_2] + k_{60d}} \quad (3)$$

$$y_1 = 1 - x_1 \quad (4)$$

We first consider the chain of reactions followed by the formation of ethyl (C_2H_5). Of importance are the reactions

$$NO + C_2H_5\dot{O}_2 \rightarrow NO_2 + C_2H_5\dot{O} \quad \text{(R9.60g)}$$

$$O_2 + C_2H_5\dot{O} \rightarrow HO_2 + CH_3CHO \quad \text{(R4.60h)}$$

$$C_2H_5\dot{O} \rightarrow HCHO + CH_3 \quad \text{(R60h)}$$

The relative importance x_2 of reaction R4.60h, compared to y_2 of reaction R60h, is given by

$$x_2 = \frac{k_{4\cdot 60h} \cdot [O_2]}{k_{4\cdot 60} \cdot [O_2] + k_{60h}} \quad (5)$$

$$y_2 = 1 - x_2 \quad (6)$$

We will underline that the ratios x_1, y_1, x_2, and y_2 are independent of the degree of pollution. Ethylmethylketone ($CH_3COC_2H_5$), which has a photochemical lifetime of several hours, may at times build up to considerable amounts. It is partly lost through photodissociation:

$$CH_3COC_2H_5 + h\nu \rightarrow CH_3CO + C_2H_5 \quad \text{(R60e.h}\nu\text{)}$$

and partly through reaction with hydroxyl:

$$HO + CH_3COC_2H_5 \rightarrow H_2O + CH_3CO\dot{C}HCH_3 \quad \text{(R19.60e)}$$

The contribution of CH_3CO and C_2H_5 to the formation of pollution products has been discussed previously, while the formation of $CH_3CO\dot{C}HCH_3$ is followed by reactions leading to $NO \rightarrow NO_2$ conversion and to production of HO_2 and CH_3CO:

$$NO + CH_3COCH(\dot{O}_2)CH_3 \rightarrow NO_2 + CH_3COCH(\dot{O})CH_3 \quad \text{(R9.60j)}$$

$$O_2 + CH_3COCH(\dot{O})CH_3 \rightarrow HO_2 + CH_3COCOCH_3 \quad \text{(R4.60k)}$$

$$CH_3COCOCH_3 + h\nu \rightarrow 2CH_3CO \quad \text{(R60s.h}\nu\text{)}$$

Biacetyl ($CH_3COCOCH_3$) is an intermediate compound with a lifetime of 1–2 hours with respect to photodissociation.

We now turn to the description of the main features of the chain of reactions following the formation of *n*-butyl (nC_4H_9).

Conversion of NO to NO_2 takes place through the reaction

$$NO + nC_4H_9\dot{O}_2 \rightarrow NO_2 + nC_4H_9\dot{O} \quad \text{(R9.60n)}$$

leading further to the production of formaldehyde through the reaction

$$nC_4H_9\dot{O} \rightarrow HCHO + nC_3H_7 \quad \text{(R60o)}$$

The decomposition of *n*-propyl (nC_3H_7) is analogous to the decomposition of *n*-butyl, with conversion of NO to NO_2 and production of formaldehyde:

$$NO + nC_3H_7\dot{O}_2 \rightarrow NO_2 + nC_3H_7\dot{O} \quad \text{(R9.60q)}$$

$$nC_3H_7\dot{O} \rightarrow HCHO + C_2H_5 \quad \text{(R60r)}$$

The reaction scheme used in this work for the decomposition of *n*-butane is listed in Table 5.

n-hexane oxidation

It is assumed that the main loss of *n*-hexane occurs through reaction with hydroxyl. By analogy with paraffins of lower order we suggest the following sequence of reactions:

$$HO + nC_6H_{14} \rightarrow H_2O + \text{sec } C_6H_{13} \quad \text{(R19.62a)}$$

$$O_2 + \text{sec } C_6H_{13} \rightarrow \text{sec } C_6H_{13}\dot{O}_2 \quad \text{(R4.62b)}$$

$$NO + \text{sec } C_6H_{13}\dot{O}_2 \rightarrow NO_2 + \text{sec } C_6H_{13}\dot{O} \quad \text{(R9.62c)}$$

$$\text{sec } C_6H_{13}\dot{O} \rightarrow CH_3CHO + \text{sec } C_4H_9 \quad \text{(R62d)}$$

(The notation sec C_6H_{13} means $CH_3\dot{C}HCH_2CH_2CH_2CH_3$). The further decomposition of the products formed through reaction R62d is discussed previously in this chapter. The rate coefficient assumed for the initial reaction is an extrapolation from the rate coefficients of the lower paraffins with hydroxyl, and is estimated at 7×10^{-12} cm^3 . s^{-1} molecules^{-1}.

The compounds formed through reactions R19.62a, R4.62b, and R9.62c are assumed to be in photochemical equilibrium. (See Table 6.) Thus,

the extension from *n*-butane to *n*-hexane does not introduce any new components to be computed beside *n*-hexane, but an additional transfer of NO to NO_2 will take place through reaction R9.62c. The reaction scheme for the decomposition of *n*-hexane is given in Table 6.

5. RESULTS

In our time-dependent box models we compute the chemical development during a 4 hours' period around noon. Computations are made for 40° and 60° latitude and for three seasons: summer, winter, and spring. Separate models have been computed for the four hydrocarbons: ethylene, propylene, *n*-butane, and *n*-hexane. For each of these models we have varied the mixing ratios of nitrogen oxides and hydrocarbons within very wide limits, ranging from 10^{-9} to 10^{-4}. In all cases we have assumed as initial condition that 25% (by volume) of the nitrogen oxides (NO_x) is in the form of NO_2. Our computations show that there is a close relation between the formation of secondary pollutants, e.g. ozone, aldehydes, and PAN. If, for instance, one mixture favors ozone formation, high levels of other pollutants are likely to occur as well. If, on the other hand, ozone is unaffected or even destroyed, PAN and in general aldehydes will remain at low levels.

In order to get an overall picture of the basic requirements for development of toxic pollutants, it is therefore sufficient to analyse the formation of ozone. The first striking feature of the conditions for ozone formation is the dependence on the ratio hydrocarbon to nitrogen oxides (HC/NO_x) in the mixtures. This is demonstrated in Figure 1, which is based on a constant NO_x mixing ratio of 0·3 ppm and varying HC/NO_x ratio. For each hydrocarbon there exists a critical HC/NO_x ratio, below which ozone remains at a low level, and above

Table 5. *n*-butane oxidation scheme (same units as in Table 2*a*).

R19.60aI	$HO + nC_4H_{10} \rightarrow H_2O + \text{sec } C_4H_9$	2.0×10^{-12}
R19.60aII	$HO + nC_4H_{10} \rightarrow H_2O + nC_4H_9$	3.5×10^{-13}
R4.60b	$O_2 + \text{sec } C_4H_9 \rightarrow \text{sec } C_4H_9O_2$	6.2×10^{-12}
R9.60c	$NO + \text{sec } C_4H_9\dot{O}_2 \rightarrow NO_2 + \text{sec } C_4H_9\dot{O}$	2.9×10^{-13}
R60d	$\text{sec } C_4H_9\dot{O} \rightarrow CH_3CHO + C_2H_5$	1.2×10^{3}
R4.60d	$O_2 + \text{sec } C_4H_9\dot{O} \rightarrow HO_2 + CH_3COC_2H_5$	2.0×10^{-16}
R4.60f	$O_2 + C_2H_5 \rightarrow C_2H_5O_2$	6.2×10^{-12}
R9.60g	$NO + C_2H_5\dot{O}_2 \rightarrow NO_2 + C_2H_5O$	2.9×10^{-13}
R60h	$C_2H_5\dot{O} \rightarrow HCHO + CH_3$	3.3×10^{1}
R4.60h	$O_2 + C_2H_5\dot{O} \rightarrow HO_2 + CH_3CHO$	3.5×10^{-17}
R60e.hν	$CH_3COC_2H_5 + h\nu \rightarrow CH_3CO + C_2H_5$	$J_{CH_3COC_2H_5} = 1.4 \times 10^{-5}$
R19.60e	$HO + CH_3COC_2H_5 \rightarrow H_2O + CH_3C\dot{O}CHCH_3$	5.3×10^{-12}
R4.60i	$O_2 + CH_3C\dot{O}CHCH_3 \rightarrow CH_3COCH(\dot{O}_2)CH_3$	6.2×10^{-12}
R9.60j	$NO + CH_3COCH(\dot{O}_2)CH_3 \rightarrow NO_2 + CH_3COCH(\dot{O})CH_3$	2.9×10^{-13}
R4.60k	$O_2 + CH_3COCH(\dot{O})CH_3 \rightarrow HO_2 + CH_3COCOCH_3$	2×10^{-16}
R60s.hν	$CH_3COCOCH_3 + h\nu \rightarrow 2CH_3CO$	$J_{CH_3COCOCH_3} = 1.7 \times 10^{-4}$
R4.60m	$O_2 + nC_4H_9 \rightarrow nC_4H_9O_2$	6.2×10^{-12}
R9.60n	$NO + nC_4H_9\dot{O}_2 \rightarrow NO_2 + nC_4H_9\dot{O}$	2.9×10^{-13}
R60o	$nC_4H_9\dot{O} \rightarrow HCHO + nC_3H_7$	3.1×10^{3}
R4.60p	$O_2 + nC_3H_7 \rightarrow nC_3H_7\dot{O}_2$	6.2×10^{-12}
R9.60q	$NO + nC_3H_7\dot{O}_2 \rightarrow NO_2 + nC_3H_7\dot{O}$	2.9×10^{-13}
R60r	$nC_3H_7\dot{O} \rightarrow HCHO + C_2H_5$	3.1×10^{3}

Table 6. *n*-hexane oxidation scheme (same units as in Table 2*a*).

R19.62a	$HO + nC_6H_{14} \rightarrow H_2O + \text{sec } C_6H_{13}$	7×10^{-12}
R4.62b	$O_2 + \text{sec } C_6H_{13} \rightarrow \text{sec } C_6H_{13}O_2$	6.2×10^{-12}
R9.62c	$NO + \text{sec } C_6H_{13}\dot{O}_2 \rightarrow NO_2 + \text{sec } C_6H_{13}\dot{O}$	2.9×10^{-13}
R62d	$\text{sec } C_6H_{13}\dot{O} \rightarrow CH_3CHO + \text{sec } C_4H_9$	1.2×10^{3}

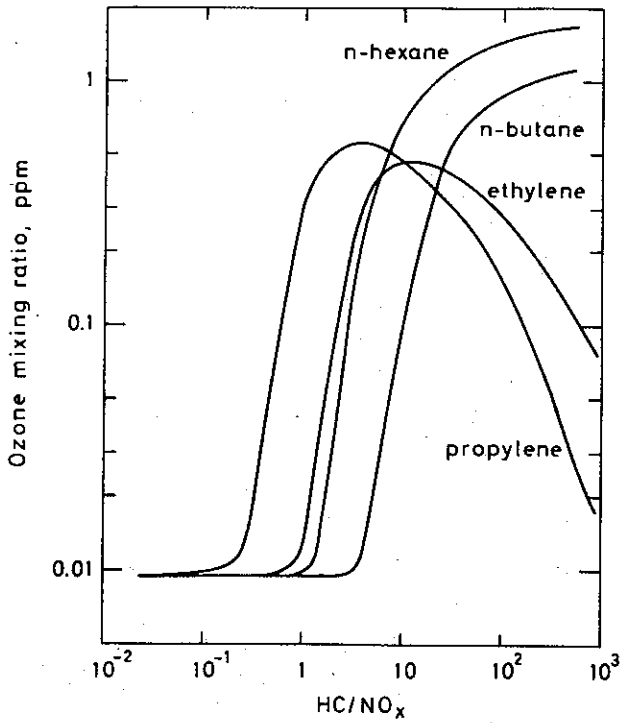

Fig. 1. Maximum ozone mixing ratios in mixtures of air, nitrogen oxides, and hydrocarbons during a four hour period around noon at 40°N latitude, summer, as a function of the initial HC/NO_x mixing ratio. The initial NO_x mixing ratio is 0.3 ppm. (Results for 0.1 and 1 ppm are almost identical and are therefore not shown.)

which ozone is formed in concentrations exceeding atmospheric background values. For propylene, which is the most reactive of the four hydrocarbons we consider, ozone is formed for HC/NO_x ratios as low as 1:2. However, for *n*-butane the critical HC/NO_x ratio is about ten times higher.

When the HC/NO_x ratio exceeds the critical value, even small perturbations will alter the ozone formation considerably. In actual pollution cases the HC/NO_x ratio is often close to the critical value, and it is therefore important to keep this ratio as low as possible.

For high values of the HC/NO_x ratio, olefins and paraffins behave differently with respect to ozone formation. When olefins are considered, ozone is suppressed through reactions R7.57a and R7.59a. We find that the ozone formation is strongest for HC/NO_x ratios around 5:1. Such a maximum does not exist for paraffins because they are assumed not to react with ozone.

A more detailed description of the ozone formation is given in Figures 2–5, where, in contrast to Figure 1, also the NO_x content is varied over a wide range. The dependence on season and lati-

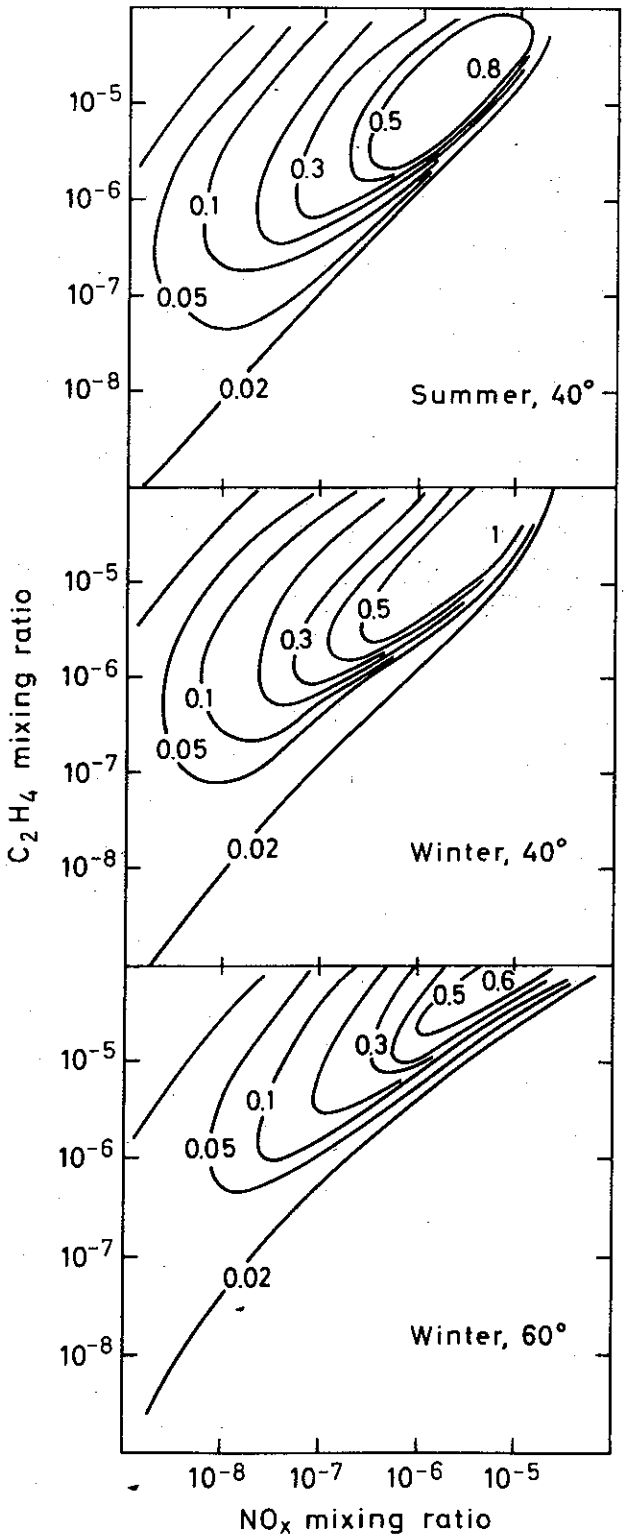

Fig. 2. Maximum ozone mixing ratios (in ppm) during a four hour period around noon in mixtures of air, nitrogen oxides, and ethylene, as a function of the initial C_2H_4 and NO_x mixing ratios.

tude is accounted for by appropriate variation in solar fluxes and temperature. Calculations are made for all seasons at 40° and 60° N latitude. The

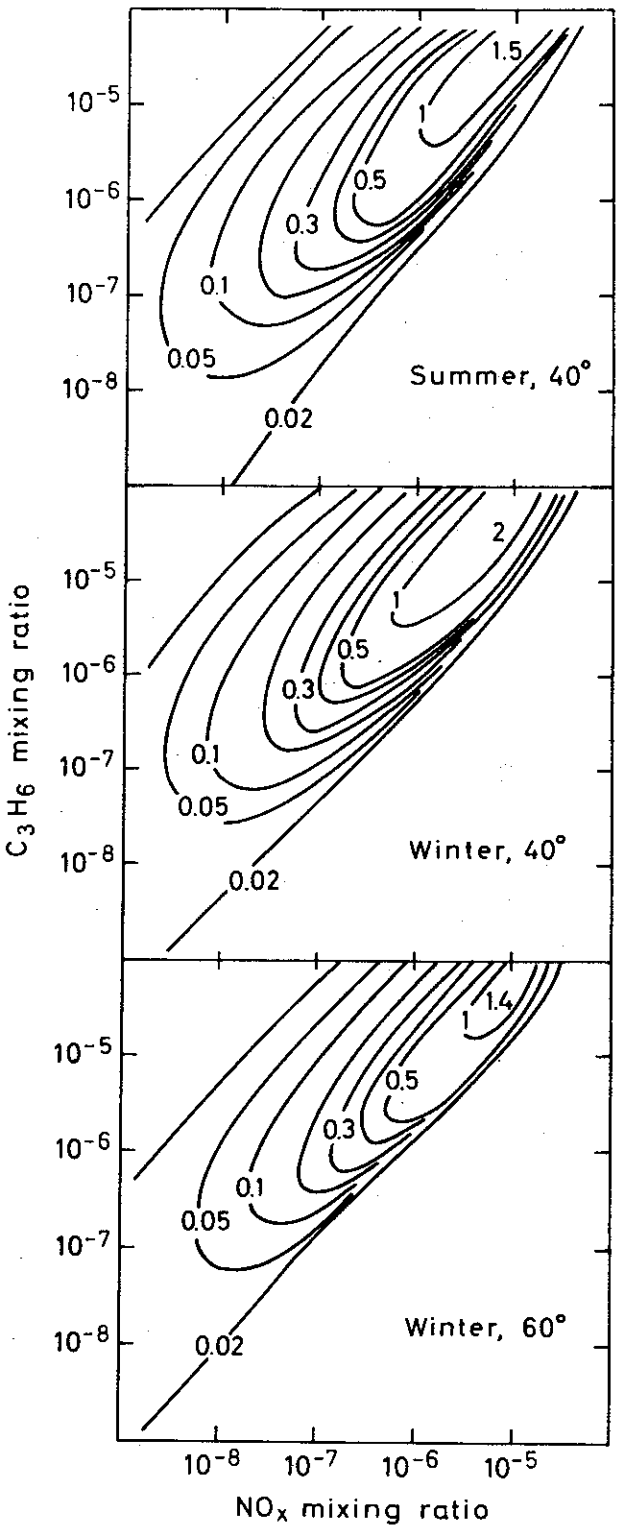

Fig. 3. Maximum ozone mixing ratios (in ppm) during a four hour period around noon in mixtures of air, nitrogen oxides, and propylene, as a function of the initial C_3H_6 and NO_x mixing ratios.

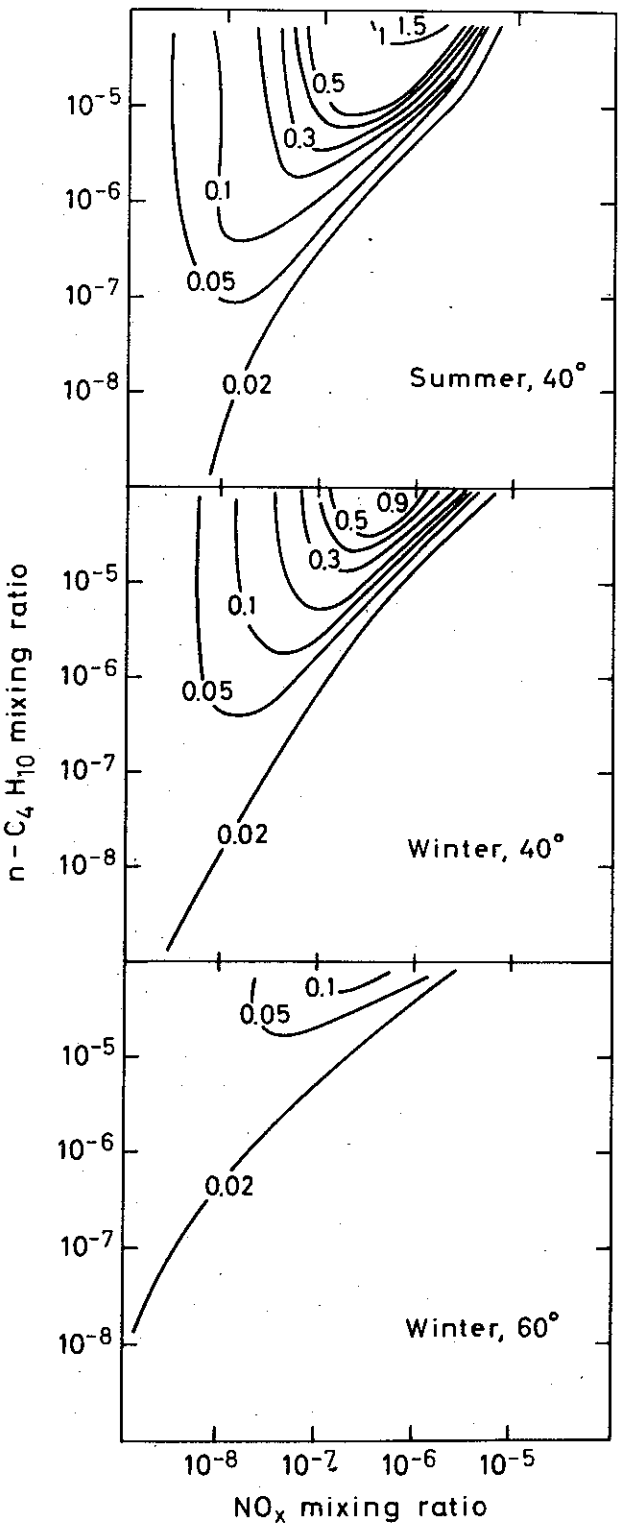

Fig. 4. Maximum ozone mixing ratios (in ppm) during a four hour period around noon in mixtures of air, nitrogen oxides, and *n*-butane, as a function of the initial nC_4H_{10} and NO_x mixing ratios.

ozone field during spring and fall differs only insignificantly from the summer-picture, and is not shown in the figure. Similarly, the calculations for

summer conditions at 60°N latitude are not presented because of their close resemblance to the results for 40°N latitude, summer.

The annual variations in the ozone field are different for olefins compared to paraffins. At 40°N latitude, the ozone formation in olefin mixtures varies little with season, while the ozone maximum is significantly reduced in the winter for paraffins. As we enter winter, at 60°N latitude, the ozone field is considerably flattened for all hydrocarbons in question.

Although the ozone maxima are less pronounced during winter at 60°N latitude when ethylene and propylene mixtures are considered, ozone may in certain cases exceed limits recommended for human exposure (OECD 1975).

This discussion shows that a certain minimum of solar radiation is required for ozone formation; above this minimum value, ozone depends only insignificantly on the intensity of sunlight. Hence, except for winter conditions when the radiation is strongly reduced at 60°N latitude, the problem of oxidant formation may be as severe at this latitude as at lower latitudes.

It is an interesting result of our model calculations that although the initial decomposing reactions proceed slower for paraffins than they do for olefins with the same number of carbon atoms, their ability to form ozone when mixed with nitrogen oxides is quite analogous. This becomes even more significant when pollutants are allowed to build up on a time scale of days, so that paraffins may accumulate due to slower loss rates. This point is often overlooked when hydrocarbons are classified as 'active' olefins and 'inactive' paraffins. We further find that the difference in ozone formation within the olefin or paraffin groups of compounds is less pronounced (mainly due to the reactivity of the hydrocarbon in question) than the difference between various olefins and paraffins. This means that, although hydrocarbon emissions usually consist of a large number of species, it is possible to represent these, as a first approximation, by a few olefins and paraffins, according to the reactivity of the emitted compounds.

The formation of other pollutants (H_2O_2, HCHO, CH_3CHO, and PAN) is also strongly dependent on the HC/NO_x ratio. In general, the same ratios that favor ozone formation, also favor the formation of other pollutants, even though

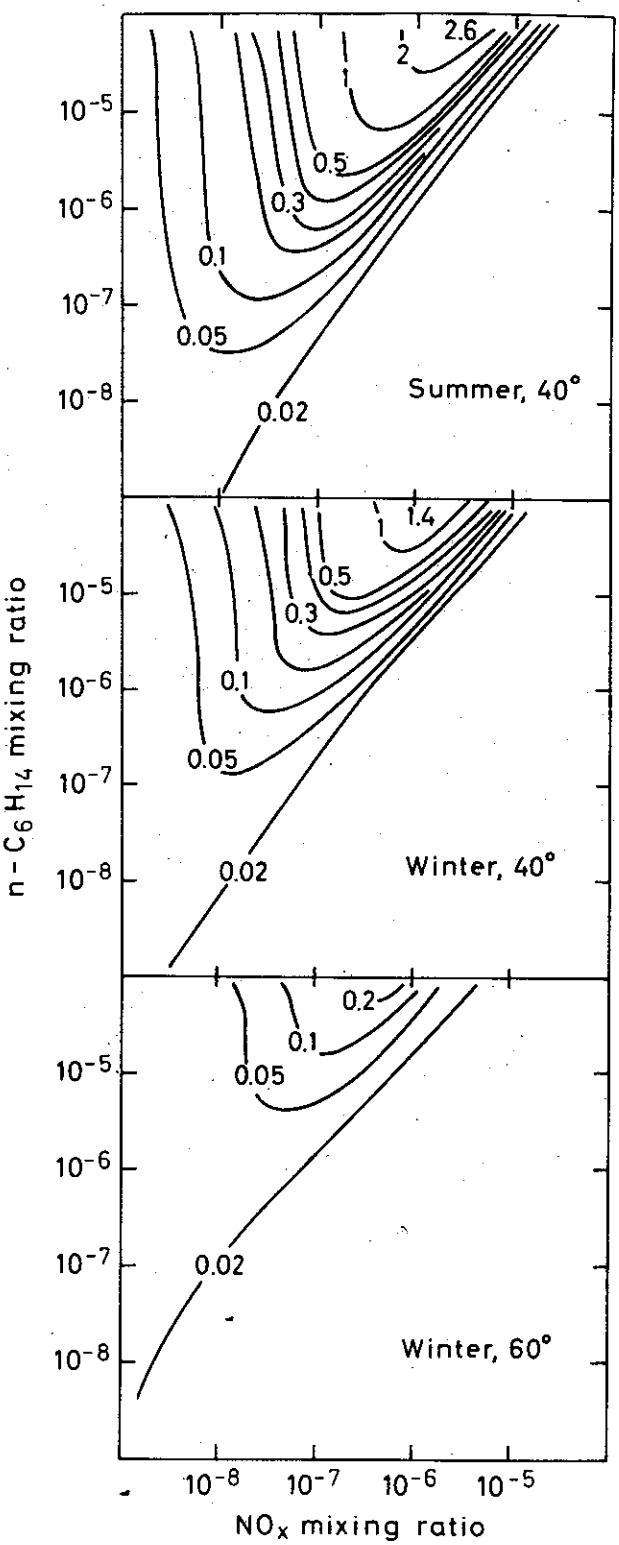

Fig. 5. Maximum ozone mixing ratios (in ppm) during a four hour period around noon in mixtures of air, nitrogen oxides, and *n*-hexane, as a function of the initial nC_6H_{14} and NO_x mixing ratios.

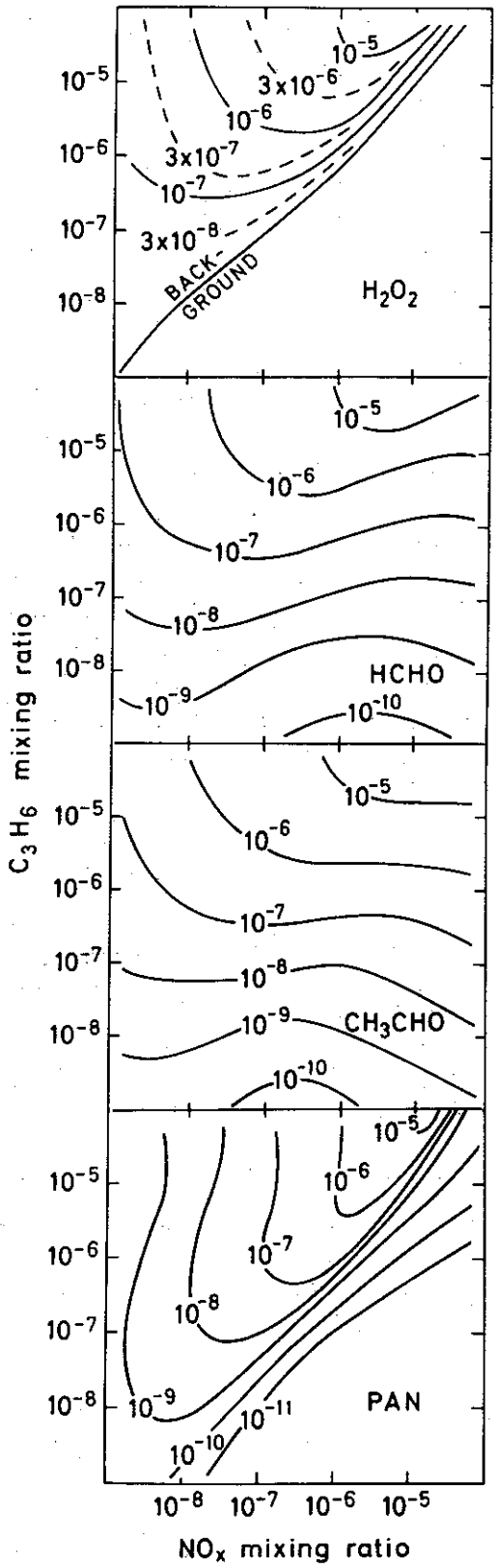

Fig. 6. Mixing ratios of hydrogen peroxide, formaldehyde, acetaldehyde, and PAN obtained in four hours in mixtures of air, nitrogen oxides, and propylene, as a function of the initial C_3H_6 and NO_x mixing ratios (noon conditions at 40°N latitude, summer).

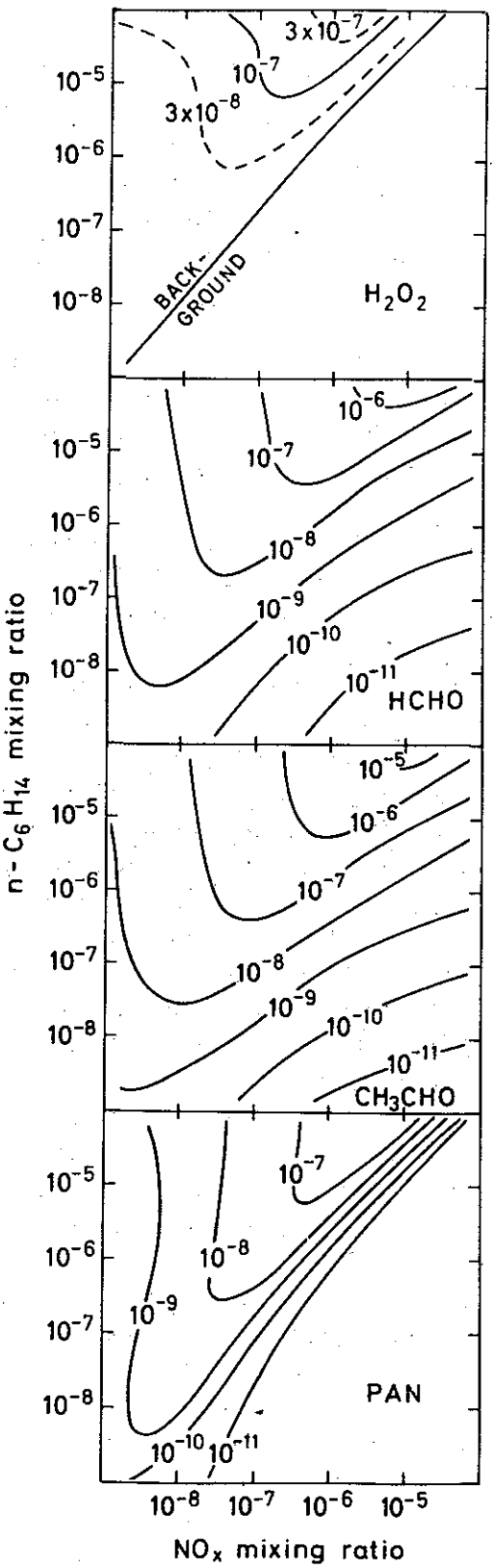

Fig. 7. Mixing ratios of hydrogen peroxide, formaldehyde, acetaldehyde, and PAN obtained in four hours in mixtures of air, nitrogen oxides, and *n*-hexane, as a function of the initial nC_6H_{14} and NO_x mixing ratios (noon conditions at 40°N latitude, summer).

there are differences between the various hydrocarbons. Again, the most pronounced differences are found between olefins and paraffins. Figures 6 and 7 show the maximum densities of hydrogen peroxide, formaldehyde, acetaldehyde, and PAN, with propylene as olefin and *n*-hexane as paraffin.

For hydrogen peroxide the analogy with ozone is obvious, but the variations with the HC/NO_x ratio are more pronounced for propylene. For an optimal HC/NO_x ratio, the density of hydrogen peroxide may increase by a factor 1000 compared to the value 0·01 ppm of the background atmosphere. For *n*-hexane the hydrogen peroxide levels are much lower.

The large differences between olefins and paraffins arise from the differences in HO_2; the production of hydrogen peroxide is proportional to the square of $[HO_2]$.

With respect to formaldehyde and acetaldehyde formation, the pictures are quite similar to the ozone diagrams for HC/NO_x ratios larger than one. However, propylene is seen to favor the formation of aldehydes even for HC/NO_x ratios much less than one. This can be explained by the fact that large NO_x densities favor production of atomic oxygen through photodissociation of nitrogen dioxide. In such cases olefins will effectively be broken down by reactions with atomic oxygen although hydroxyl remains at a low level.

The diagrams for PAN show essentially the same features as we found for ozone. The difference between propylene and *n*-hexane is pronounced. Propylene is an efficient producer of PAN; *n*-hexane will hardly produce PAN levels of concern.

In order to demonstrate how the main features in the time evolvement of the chemistry may proceed quite differently in spite of relatively small changes in the mixing ratios of hydrocarbons and nitrogen oxides, two cases of different HC/NO_x ratio are selected. Both computations are for propylene, 40° latitude, summer. In the first case ('active' mixture) we have assumed 1 ppm for the propylene mixing ratio and 0·3 ppm for the NO_x mixing ratio. In the second case ('inactive' mixture) we have assumed 0·3 ppm for the propylene mixing ratio and 1 ppm for the NO_x mixing ratio. The time evolvement during a four-hour period of propylene and its end products is shown in Figures 8 and 9. Formaldehyde and acetaldehyde are summed up in Figure 8 because they follow each other closely.

In the 'active' mixture, all components show drastic changes in density over the time period we consider. The propylene content is reduced by a factor ten, approximately. The densities of end products such as carbon monoxide, aldehydes, and hydrogen peroxide show an increase as a result of the decreasing propylene concentration. Characteristic of an 'active' mixture is a substantial transfer of the initial hydrocarbon to the end products.

Another essential feature of an 'active' mixture is also demonstrated: the complete conversion of nitric oxide to nitrogen dioxide and other nitrogen compounds. This conversion determines the rate of ozone formation. It is further apparent from Figure 9 that peroxyacetyl nitrate (PAN) builds up more slowly than other pollutants, but after

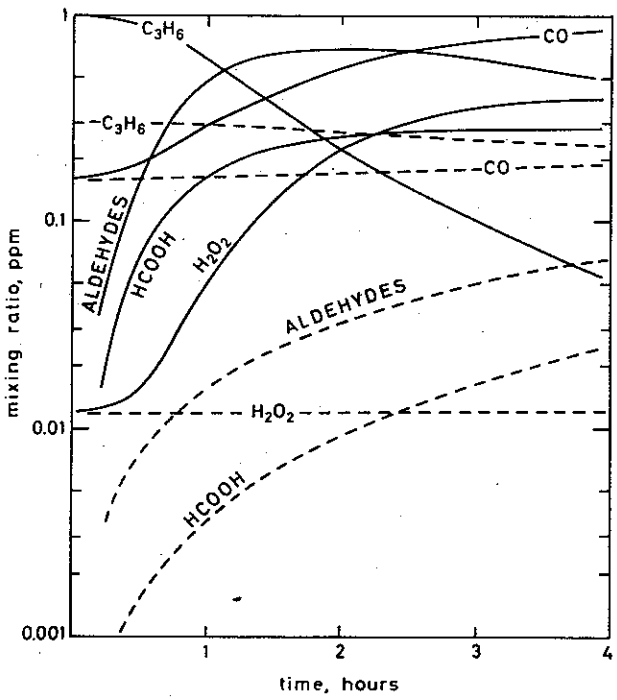

Fig. 8. Mixing ratios of propylene, carbon monoxide, aldehydes (the sum of formaldehyde and acetaldehyde), formic acid, and hydrogen peroxide as a function of time (noon conditions, 40°N latitude, summer). Full lines refer to an 'active' mixture (initial mixing ratios: 1 ppm for propylene, 0.3 ppm for nitrogen oxides), while dashed lines refer to an 'inactive' mixture (initial mixing ratios: 0.3 ppm for propylene, 1 ppm for nitrogen oxides).

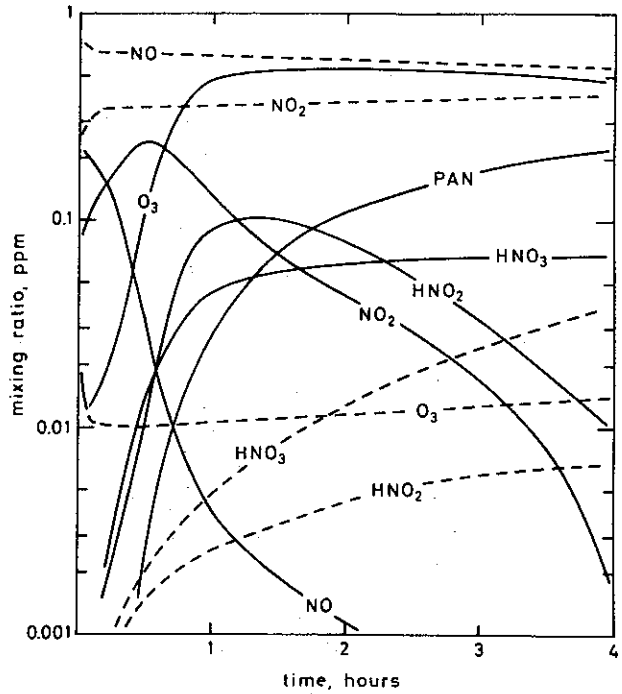

Fig. 9. Mixing ratios of nitrogen oxide, nitrogen dioxide, ozone, nitrous acid, nitric acid, and PAN as a function of time (noon conditions, 40°N latitude, summer). Full lines refer to an 'active' mixture (initial mixing ratios: 1 ppm for propylene, 0.3 ppm for nitrogen oxides), while dashed lines refer to an 'inactive' mixture (initial mixing ratios: 0.3 ppm for propylene, 1 ppm for nitrogen oxides).

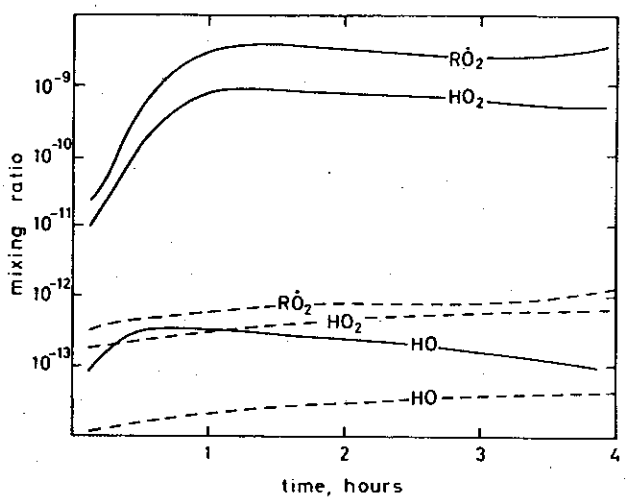

Fig. 10. Mixing ratios of hydroxyl, hydrogen dioxide, and radicals of the form $R\dot{O}_2$ (the sum of CH_3O_2, $\overline{CH_2CH(\dot{O}_2)CH_2O\dot{O}}$, and $CH_3CH(\dot{O}_2)CH_2OH$), as a function of time at 40°N latitude, summer. Full lines refer to an 'active' mixture of air, propylene, and nitrogen oxides, while dashed lines refer to an 'inactive' mixture.

1–2 hours the densities are comparable. In fact, after 4 hours PAN is the most abundant nitrogen contaminant (0·15 ppm), leading to a reduction in the densities of other nitrogen species (NO_x, HNO_2).

Special attention should be paid to hydrogen peroxide and nitrous acid. These compounds may act as important sources of hydroxyl in the initial phase of time integration (R23.hν, R25.hν) if they are present in high concentrations due to pollution. In the calculations presented here, background concentrations are assumed as initial conditions for hydrogen peroxide and nitrous acid.

The time evolvement of the 'inactive' mixture shows a striking contrast to the 'active' mixture. Only a minor reduction in the propylene concentration has taken place, causing a very slow increase in the densities of secondary pollutants. Aldehydes do not reach levels of concern after 4 hours (<0·05 ppm); the same is the case for ozone and hydrogen peroxide which do not exceed their background values. The transfer of nitric oxide to nitrogen dioxide is very slow; nitric oxide is the most abundant nitrogen compound throughout. The formation of PAN, nitrous acid, and nitric acid is negligible.

The fundamental differences between 'active' and 'inactive' mixtures, shown here for propylene, are also found for the other hydrocarbons, although the time evolvement may be somewhat slower due to slower initial loss rates. Furthermore, the borderlines between 'active' and 'inactive' mixtures are defined by higher HC/NO_x ratios than for propylene.

The large differences between 'active' and 'inactive' mixtures are determined by the efficiency of the nitric oxide to nitrogen dioxide conversion through radical reactions. To demonstrate this effect, concentrations have been computed for HO_2 and radicals of the form $R\dot{O}_2$ in the 'active' and 'inactive' case, with propylene as hydrocarbon. The calculation of radicals of the form $R\dot{O}_2$ is in general omitted because they are assumed to be in a state of photochemical equilibrium, but is included in this context in order to show their importance in the nitric oxide to nitrogen dioxide conversion. The results are shown in Figure 10.

The time evolvement and concentrations ob-

tained for HO_2 and $R\dot{O}_2$ seem to follow each other closely in both mixtures. However, there is a three-order of magnitude increase in their concentrations in the 'active' compared to the 'inactive' mixture. This demonstrates the fundamental differences in the two mixtures, indicating HO_2 and radicals of the form $R\dot{O}_2$ as keys to whether pollutants are formed or not.

On the other hand, hydroxyl shows a less marked dependence on the ratio HC/NO_x because its density is directly controlled by the amount of hydrocarbons released. This is apparent from Figure 10.

APPENDIX

Computational methods

The time evolution of the component X is described by the differential equation

$$\frac{\partial[X]}{\partial t} = P_X - Q_X[X] \qquad \text{(A.1)}$$

where P_X is the production and $Q_X[X]$ is the loss rate of the component X.

P_X and Q_X do not have $[X]$ as a factor, but may in many cases be implicit functions of $[X]$. Depending on the chemical lifetime of the component considered, different solutions of equation (A.1) are applied. With lifetimes longer than 1000 s a simple linear expansion is used (Euler's method):

$$[X]_{t+\Delta t} = [X]_t + (P_{X,t} - Q_{X,t}[X]_t) \cdot \Delta t \qquad \text{(A.2)}$$

where Δt is the timestep. In the computations presented here, a time step of 10 s has been used. However, the error introduced by increasing the time step to 30 s turns out to be insignificant.

Components with lifetimes between 1 s and 1000 s are computed by the explicit solution

$$[X]_{t+\Delta t} = [X]_e + ([X]_t - [X]_e) \exp(-Q_X \Delta t) \qquad \text{(A.3)}$$

where $[X]_e$ denotes the photochemical equilibrium expression

$$[X]_e = P_X/Q_X \qquad \text{(A.4)}$$

Components with short chemical lifetimes (shorter than 1 s) are computed according to the equilibrium equation (A.4).

Components whose concentrations are computed according to the solutions (A.2) and (A.3) require specification of initial conditions, and these are assumed to be the atmospheric background values: $[O_3] = 5 \times 10^{11}$, $[H_2O_2] = 3 \times 10^{11}$, $[HO_2] = 8 \times 10^7$, $[CO] = 4 \times 10^{12}$, $[HCHO] = 4.5 \times 10^9$, $[HNO_2] = 2.5 \times 10^8$, $[HNO_3] = 1.0 \times 10^9$ (unit: molecules . cm^{-3}).

The water vapor concentration is computed assuming 75% relative humidity. The mixing ratio of methane is assumed constant 1·4 ppm. Components not present in the background atmosphere (derivatives of the hydrocarbon oxidation) are given zero concentration as initial condition.

REFERENCES

Ackerman, M. 1971. p. 149 in *Mesospheric Models and Related Experiments* (ed. by G. Fiocco). D. Reidel Publishing Company, Dordrecht, Holland.

Chameides, W. 1975. *J. Geophys. Res. 80*, 4989–4996.

Crutzen, P. 1973. *Pure Appl. Geophys.*, 106–108, 1385–1399.

Crutzen, P. J., Isaksen, I. S. A. & McAffe, J. 1976. *J. Geophys. Res.* (in press).

Demerjian, K. L., Kerr, J. A. & Calvert, J. G. 1974. Chapter 1 in *Adv. Environ. Sci. Technol. 4.*

Fabian, P. & Junge, Chr. E. 1970. *Arch. Met. Geoph. Biokl.*, Ser. A, *19*, 161–172.

Hampson, R. F., Jr. & Garvin, D. 1975. U.S. Department of Commerce, National Bureau of Standards, Technical Note 866, June 1975.

Hampson, R. F. 1973. *J. Phys. Chem. Ref. Data 2*, 267–312.

Hesstvedt, E. 1975. *Geophys. Norv. 31*, No. 2.

Hesstvedt, E. & Isaksen, I. S. A. 1974. Report No. 6, Institutt for Geofysikk, Universitetet i Oslo.

Hov, Ø. 1975. Thesis for the Master's Degree, Universitetet i Oslo (in Norwegian).

Isaksen, I. S. A. & Crutzen, P. J. 1976. *Geophys. Norv. 31*, No. 4.

Isaksen, I. S. A., Midtbø, K. H., Sunde, J. & Crutzen, P. J. 1976. Report No. 20, Institutt for Geofysikk, Universitetet i Oslo.

Johnston, H. S. 1973. Quarterly Progress Report, March–June 1973. CIAP.

Levy, H. 1971. *Science 1973*, 141.

Lin, C. L. & DeMore, W. B. 1973. *J. Photochem. 2*, 161–164.

Moortgat, G. K. & Warneck, P. 1975. *Z. Naturforsch. 30a*, 835–844.

OECD, Air Management Sector Group 1975. pp. 37–39 in *Photochemical Oxidant Air Pollution*. OECD, Paris, 1975.

Instructions to Authors

GEOPHYSICA NORVEGICA

publishes papers in English. When preparing manuscripts for submission, authors should consult current copies of the journal and follow its style as closely as possible.

MANUSCRIPTS

Manuscript must be typewritten, double spaced throughout, on one side of the paper, with a wide margin. Authors should submit the *original* manuscript (preferably with one copy) to the editor, whose address is shown on page 2 of the cover.

Separate sheets should be used for the following: 1) title page, with the author's name and institution, and, if the title is longer than 40 letters and spaces, a short title not exceeding this limit for use in the running heads; 2) an abstract not exceeding 12 lines (910 letters and spaces) with the name and full postal address underneath of the author to whom communications, proofs, and reprints are to be sent; 3) references; 4) Tables with their headings; 5) legends to Figures.

Brief *Acknowledgements* of grants and other assistance, if any, will be printed at the end of the text.

FIGURES, TABLES, AND MATHEMATICAL SYMBOLS

All illustrations are to be considered as Figures. Each graph, drawing, or photograph should be numbered in sequence with arabic numerals, and should be identified on the back by the name of the journal, the author's name, and the Figure number. The top should be indicated. The Figures should be the original drawing. The columns of *Geophysica Norvegica* are 67 mm broad, and the size of the original drawings should be in proportion. Lines must be thick enough to allow for reduction. Letters and numbers should not be less than 2 mm high in the printed illustration. Photographs should be submitted as unmounted glossy enlargements showing good details.

Tables are to be numbered consecutively. Each Table should be typed on a separate sheet, with a descriptive heading that makes the Table self-explanatory.

All Figures and Tables should be referred to in the text by their number. Their approximate position should be indicated in the margin of the manuscript.

All numbered equations and all unnumbered but complicated equations should be typed on separate lines. Equations should be punctuated.

All text material will be set in roman type unless otherwise marked. Hence, all variables and other characters to be set in italic type should be underlined once with a straight line. Vectors and other characters in boldface type should be indicated by underlining with a single wavy line.

No footnotes should be used.

REFERENCES TO LITERATURE

In the text, Brown (1957, p. 9), Brown & White (1961). If more than two authors, Brown et al. (1963). Multiple references: 'As several authors have reported (Brown 1967, Brown & White 1961, Green et al. 1963)', i. e. chronological order, no commas between names and year.

Lists of References are to be unnumbered and in alphabetical order. The international alphabetical order of Scandinavian and German vowels, should be observed: Å = AA, Æ and Ä = AE, Ø and Ö = OE, Ü = UE. Indicate 1st, 2nd, 3rd, etc. works by the same author in the same year by a, b, c, etc. (White 1966a). No ditto marks should be used. Titles of journals should be abbreviated according to *World List of Scientific Periodicals.*

Examples:

Cadle, R. D. 1966. p. 83 in *Particles in the Atmosphere and Space.* Reinhold Publishing Corporation, New York.

Craig, R. A. 1965. p. 161 in *The Upper Atmosphere. Meteorology and Physics.* International Geophysics Series, Vol. 8. Academic Press, New York and London.

Eliassen, A. & Kleinschmidt, E. 1957. p. 66 in *Handbuch der Physik.* Vol. 48, Part 2, edited by S. Flügge. Springer-Verlag, Berlin.

Junge, C. 1972. *Quart. J. R. Met. Soc. 98,* 711.

PROOFS

Two copies of the first proof will be sent (page proofs). One copy, duly corrected, should be returned to the editor with the least possible delay. All technical parts of the article, including references, names, figures (numbers, formulae), illustrations, etc. are the responsibility of the authors. Authors will be required to pay for any major alterations they may make.

REPRINTS

Fifty reprints of each article will be supplied free. Additional reprints can be ordered at a charge.